BAR-based Multi-dimensional Nonequilibrium Pulling for Indirect Construction of QM/MM Free Energy Landscape

Xiaohui Wang[1,2], Qiaole He[3,4], and Zhaoxi Sun[1,3*]

[1]*State Key Laboratory of Precision Spectroscopy, School of Chemistry and Molecular Engineering, East China Normal University, Shanghai 200062, China*

[2]*Institute of Computational Science, Università della Svizzera italiana (USI), Via Giuseppe Buffi 13, CH-6900, Lugano, Ticino, Switzerland*

[3]*Computational Biomedicine (IAS-5/INM-9), Forschungszentrum Jülich, Jülich 52425, Germany, and Forschungszentrum Jülich GmbH, IBG-1: Biotechnology, Wilhelm-Johnen-Str. 1, 52425 Jülich, Germany*

[4]*State Key Laboratory of Bioreactor Engineering, R&D Center of Separation and Extraction Technology in Fermentation Industry, East China University of Science and Technology, Shanghai 200237, China*

*To whom correspondence should be addressed: proszx@163.com

Abstract

Construction of free energy landscapes at Quantum mechanics (QM) level is computationally demanding. As shown in previous studies, by employing an indirect scheme (i.e. constructing a thermodynamic cycle connecting QM states via an alchemical pathway), simulations are converged with much less computational burden. The indirect scheme makes QM/ molecular mechanics (MM) free energy simulation orders of magnitude faster than the direct QM/MM schemes. However, the indirect QM/MM simulations were mostly equilibrium sampling based and the nonequilibrium methods were merely exploited in one-dimensional alchemical QM/MM end-state correction at two end states. In this work, we represent a multi-dimensional nonequilibrium pulling scheme for indirect QM/MM free energy simulations, where the whole free energy simulation is performed only with nonequilibrium methods. The collective variable (CV) space we explore is a combination of one alchemical CV and one physically meaningful CV. The current nonequilibrium indirect QM/MM simulation method can be seen as the generalization of equilibrium perturbation based indirect QM/MM methods. The test systems include one backbone dihedral case and one distance case. The two cases are significantly different in size, enabling us to investigate the dependence of the speedup of the indirect scheme on the size of the system. It is shown that the speedup becomes larger when the size of the system

becomes larger, which is consistent with the scaling behavior of QM Hamiltonians.

Introduction

Free energy differences between different states of a system or different systems of interest are of great importance in various scientific fields.[1-4] The free energy profile or the free energy landscape depicts the variation of the free energy along generalized coordinates. From these curves or surfaces, we can obtain insights about various properties of the system of interest, such as the relative stability of different states and the rate constants of transitions between them. Accurate and precise estimation of free energy landscapes requires converged phase space sampling and accurate description of the system. The sampling efficiency can be enhanced with enhanced sampling techniques, which often give several orders of magnitude speedup compared with brute force simulations.[5-8] As free energy is a state function, the free energy difference between different states can be calculated with any pathway one constructs, as long as the end states connected by the pathway remain unchanged. If the pathway is non-physical, the method is referred to as the alchemical method. The design of the alchemical pathway aims at making complex transformation feasible.[9-13] For instance, to investigate the binding/unbinding of protein-ligand complex we need to identify physically meaningful collective variable (CV) describing the important slow motions in this process. In complex systems, this is not an easy task and a lot of trails and errors are required before we reach the correct answer. By contrast, the alchemical pathway directly connects the two end states (i.e. the bound state and the unbound state) and the generalized CV, the alchemical order parameter, is used to describe the variation of Hamiltonian along the alchemical pathway. A series of intermediate states described with artificial Hamiltonians are introduced to enhance the convergence of the simulation. The alchemical method has been successfully applied to a series of cases, such as the relative binding affinity of protein-ligand complex,[14-15] solvation free energy,[14, 16] and pKa shift calculation.[17] The drawback of the alchemical method is that only the free energy difference can be obtained, and how the reaction happens in the real world remains uncovered. To get a better understanding of the behavior of the system in the real physical world, the free energy landscape along the physically meaningful CVs is required.

According to the simulation protocol and the reweighting estimators used to recover the unbiased data, the free energy simulation frameworks can be divided into equilibrium and nonequilibrium techniques. [18] In the alchemical space, examples of the equilibrium schemes are thermodynamic integration (TI)[9-11] and free energy perturbation (FEP), while in the physically meaningful CV space there are umbrella sampling[7, 19-21] and replica exchange methods.[22-27] In umbrella sampling, biasing potentials are added to enhance the sampling in specific regions in the phase space and the data obtained in the biased ensembles are reweighted to recover the distribution in the original unperturbed ensemble. In the replica exchange method, the configurations under different Hamiltonians are attempted to exchange periodically to enhance barrier crossing and conformational search. The nonequilibrium scenarios are based on the estimators of Jarzynski's Identity (JI)[28] and Crooks' Equation (CE).[29] The statistical nature of JI makes it less efficient

than CE.[30-33] Coupling these estimators with enhanced sampling methods gives the steered MD (SMD) method, where the system is pulled from the one state to another and the free energy profile is recovered with nonequilibrium works.[30, 34-37] In essence, nonequilibrium techniques are generalizations of equilibrium methods. Equilibrium methods such as FEP can be seen as the instantaneous perturbation limit of JI derivatives.

With converged statistics from the simulation, the rest of the problem lies in the accuracy of description of the system (i.e. the Hamiltonian). Quantum mechanics (QM) Hamiltonians are more accurate than molecular mechanics (MM). However, QM methods are often computationally demanding and even prohibitive for large systems such as biomolecules.[38-40] Thus, the free energy simulation with full QM treatment of the system is too slow and is affordable only for small systems in the gas phase. Multiscale simulation techniques extend the applicability of QM Hamiltonians. QM/MM and fragmentation methods enable the accurate description of large systems.[38, 41-44] However, these calculations are still too expensive for converged phase space sampling. Following the alchemical idea, the indirect QM/MM scheme is introduced.[45-49] A thermodynamic cycle is constructed and the whole transformation is decomposed into relatively cheap low-level MM simulation and MM<->QM corrections at end states, as is shown in Fig. 1a. Sometimes the low-level Hamiltonian used is semi-empirical methods such as the empirical valence bond (EVB) method.[50-52] This indirect scheme can be viewed as a special type of alchemical free energy simulation, where the different states are the same system described with different Hamiltonians. The indirect regime has been employed to recover the free energy profile along physically meaningful CV and the free energy difference between different states of the same system.[45-54] The speedup of the indirect pathway is generally several orders of magnitude and shows system dependence.[55-65] The indirect scheme can be very efficient in estimating the free energy barrier in the processes involving the breaking or the formation of chemical bonds such as the enzyme reactions by coupling the direct EVB simulation and the EVB<->QM alchemical corrections.[50] In systems where only non-bonded interactions are varying, e.g. the solvation of drug-like molecules, the polarization effect can be taken into account with the indirect QM/MM scheme with the combination of the direct MM simulation and MM<->QM corrections.[66]

In the current published scientific reports, most studies employed equilibrium free energy simulation to perform the MM simulation and MM<->QM corrections. Normally, the traditional umbrella sampling was applied to construct the low-level potential of mean force (PMF) for configurational CV, and traditional FEP or its variants such as Bennett's Acceptance Ratio (BAR)[67-68] was applied for alchemical CV. Only a few studies relying on nonequilibrium simulation techniques have been reported.[37] For instance, the nonequilibrium simulations were only used for MM<->QM corrections and the reweighting estimator was JI.[37] BAR and CE are the statistically optimal estimators in equilibrium and nonequilibrium reweighting between two thermodynamic states and the difference between them is only the quantity used in self-consistent field iterations. In BAR the energy difference is used, while in CE the

nonequilibrium work is employed.

In this work, we report a general nonequilibrium framework for the indirect calculation of QM/MM free energy landscape. As the QM/MM free energy landscape is constructed, the method can be used to investigate the behavior of the system in the real world, such as the mechanism of reactions and conformational changes. The method is built on our previous BAR/CE-based adaptive sampling in nonequilibrium stratification in the alchemical[16] and configurational spaces.[69] We combine one alchemical CV and one physically meaningful CV to construct the two-dimensional (2D) CV space. 2D nonequilibrium free energy simulation is performed and the direct QM/MM free energy profile is indirectly constructed. The closure of our thermodynamic cycle is almost perfect according to numerical simulations and the statistical noise is small, although in some cases the curve fitting is needed. The computational framework is easy to apply, the resulted indirect PMF is reliable, and the speedup is dramatic. The test cases we select include one periodic dihedral case and one non-periodic distance case. The two test cases are significantly different in size, and the difference between their speedups of the indirect scheme indicates the speedup of indirect QM/MM free energy simulation depends on the size of the system.

Methodology

One dimensional SMD and CE for PMF construction. In the current research, we're dealing with 2-dimensional enhanced sampling along one configurational CV and one alchemical CV.

For configurational CVs, the nonequilibrium approach is often called SMD, where a time-dependent harmonic potential defined by Eq. (1) is imposed on the system in order to restrain and direct it to move along the CV space,[70]

$$h(\mathbf{q}) = \frac{k}{2}\left(\xi(\mathbf{q}) - \xi_0(t)\right)^2 \qquad (1)$$

, where h is the harmonic potential, ξ_0 denotes the time-dependent CV defining the configurational pathway, $\mathbf{q}$ represents the coordinate vector, ξ refers to the current value of the CV and k is the force constant of the harmonic potential. In the stiff spring limit, the need to add corrections to account for the non-fixed behavior of initial configurations vanishes.[71-73] In alchemical space, the CV moves in almost the same way. The only difference is that the alchemical CV is fixed to the desired point and varies with the pre-defined schedule. There is no fluctuation in the alchemical CV space.

Often the long transformation is decomposed into small segments to enhance the convergence of the simulation due to reduced dissipation. The distribution of work in each segment becomes narrower with stratification. We consider the whole transformation is divided into K states and there are $K-1$ segments. To ensure reliable

reweighting and accelerate convergence, we use the arguably best estimator in two-state free energy perturbation in nonequilibrium cases, CE. The dimensionless free energy difference between two states can be obtained from the asymptotically unbiased and statistically optimal estimator of CE in Eq. (2),[29, 67-68]

$$\begin{cases} \Delta A_{ij} = \ln \dfrac{\left\langle f(W_{ji}+C)\right\rangle_j}{\left\langle f(W_{ij}-C)\right\rangle_i} + C \\ C = \Delta A_{ij} + \ln(\dfrac{n_j}{n_i}) \end{cases} \tag{2}$$

, where $\langle \ldots \rangle_i$ refers to the canonical average over nonequilibrium realizations initiated from state i, W_{ij} represents the dimensionless work accumulated during the nonequilibrium pulling initiated from state i and ended in state j, n is the number of samples in each ensemble, f is the Fermi function and $\Delta A_{ij} = A_j - A_i$ represents the dimensionless free energy difference. The corresponding variance of the free energy estimator is,

$$\sigma_{ij}^2 = \frac{\mathrm{Var}\left(f_{i,j}\right)}{n_i^2 f_{i,j}^2} + \frac{\mathrm{Var}\left(f_{j,i}\right)}{n_j^2 f_{j,i}^2} \tag{3}$$

, where Var denotes the absolute variance and the definition of f_{ij} is

$$\begin{aligned} f_{ij} &= \left\langle f(W_{ij}+C_{ij})\right\rangle_i \\ f_{ji} &= \left\langle f(W_{ji}-C_{ij})\right\rangle_j \\ n_{ij} f_{ij} &= n_{ji} f_{ji} \text{ from SCF of CE} \end{aligned} \tag{4}$$

. Here j is larger than i. Practically, we often set $j = i+1$, as only the transformations between neighboring states are performed, considering the computational efficiency. As CE requires the initial configurations for nonequilibrium realization to be extracted from equilibrium ensembles, we need to perform sampling in the equilibrium ensemble and then initiate nonequilibrium transformation. We calculate the autocorrelation time of the CV we bias in each state i, τ_i, and subsample independent configurations by the statistical inefficiency $\phi_i = 1 + 2\tau_i$.

Free energy differences of multiple segments are summed to give the overall free energy difference of the whole nonequilibrium process, namely

$$\Delta A_{1K} = \sum_{i=1}^{K-1} \Delta A_{i,i+1} \tag{5}$$

$$\sigma_{1K}^2 = \sum_{i=1}^{K-1} \sigma_{i,i+1}^2 = \sum_{i=1}^{K-1} \left(\frac{\mathrm{Var}\left(f_{i,i+1}\right)}{n_i^2 f_{i,i+1}^2} + \frac{\mathrm{Var}\left(f_{i+1,i}\right)}{n_{i+1}^2 f_{i+1,i}^2} \right) \tag{6}$$

. Setting the free energy of one state as the reference, we can obtain the PMF or the free energy profile along the CV.

Adding corrections to one-dimensional free energy profile in order to obtain multi-dimensional free energy surface. When another CV orthogonal to the first CV is added, as illustrated in Fig. 1b, correction terms are added to the free energy of all states. Bidirectional arrows indicate bidirectional pulling and bidirectional reweighting with BAR. Note that in Fig. 1b, only the transformations described with solid arrows are performed due to efficiency considerations. Assuming that we construct the 1D PMF by accumulating free energy differences from an arbitrary state assumed as state 1 and the free energy of state 1 is set as zero, namely

$$A_1 = 0 \tag{7}$$

, the free energy of state k can be calculated with

$$A_k = \Delta A_{1k} = \sum_{i=1}^{k-1} \Delta A_{i,i+1} \tag{8}$$

. In the 2D space, there are K_1 states in the configurational dimension and K_2 states in the alchemical dimension. In the 2D-PMF construction, we define the free energy of configurational state k_1 at alchemical state k_2 likewise,

$$A_{k_1 k_2} = \Delta A_{k_1 1,11} + \Delta A_{k_1 k_2, k_1 1} = \sum_{i=1}^{k_1-1} \Delta A_{i,1,i+1,1} + \sum_{j=1}^{k_2-1} \Delta A_{k_1, j, k_1, j+1} \tag{9}$$

, where $\Delta A_{k_1 1,11}$ denotes the free energy difference between configurational state 1 and configurational state k_1 with alchemical control parameter at state 1. The error is propagated with the normal error propagation procedure. Although our previous nonequilibrium stratification in the alchemical space allows us to employ the staging scheme in MM<->QM correction,[16] due to the similarity of different Hamiltonians, we only perform transformations between two end alchemical states. We define $K_2 = 1$ as the MM state and $K_2 = 2$ as the QM state. Constructing the PMF along K_1 at MM level ($K_2 = 1$) and performing MM<->QM corrections at each k_1, we can obtain the indirect PMF at QM level ($K_2 = 2$).

To compare the computational cost of direct and indirect QM/MM simulation, we need to define the cost of each nonequilibrium pulling first. According to the definition, in the initial-state sampling at state i, each independent configuration requires $\phi_{\mathrm{eq},i}$ simulation time. The nonequilibrium pulling lasts for $\phi_{\mathrm{NEW},i}$. Thus the overall computational cost for each pulling simulation is

$$\phi_i = \phi_{\mathrm{NEW},i} + \phi_{\mathrm{eq},i} \tag{10}$$

. If the pulling initiated from state i is in two directions (forward and backward), $\phi_{\mathrm{NEW},i}$ should be multiplied by 2 in the above equation. As the computational costs under different Hamiltonians differ, we scale all simulation time to

the computational cost at MM level. The computational cost comparison between MM and QM levels for our test cases including the backbone dihedral in ACE-NME and the end-to-end distance in deca-alanine are given in Table 1.

Note that for non-periodic CV if the nonequilibrium realization is initiated from intermediate states, the pulling is performed in both directions (ξ increasing and ξ decreasing) while those initiated from end states are only pulled in one direction. For periodic CV transformations initiated from each state are performed in both directions. The configurational CVs that we consider include the periodic dihedral and non-periodic distance, and the alchemical CV is non-periodic.

How to define convergence in nonequilibrium simulation. Normally in nonequilibrium pulling, the convergence is checked by the removal of bias with further sampling and slower pulling speeds.[14, 16-17] The time-evolution and the size of the statistical error or uncertainty (variance or standard error) are also needed to be checked. [14, 16-17, 30] The phenomenon that identical results are obtained at different pulling speeds and from different sample sizes indicates successful bias elimination. Small enough standard error and the monotonically nonlinear dependence of the variance on the sample size suggest the same thing. In all types of free energy simulation, small enough standard error is required to define convergence. However, how small is small enough is unclear. In the results part of our manuscript, we report a new convergence criterion which relates the size of the statistical error required for convergence with the phase space overlap in nonequilibrium pulling.

Generalization of the phase space overlap in nonequilibrium pulling. Aside from the variance in each state, another quantity for convergence check is the overlap scalar proposed in Bennett's original paper.[68] We copy its original definition here as

$$O_{ij} = \int \frac{\rho_i \rho_j \mathrm{d}\mathbf{q}}{\rho_i + \rho_j} \tag{11}$$

, where the subscript ij indicates that the scalar estimates the overlap between state i and state j. The probability density $\rho_i = \frac{e^{-U(\mathbf{q})_i}}{\int e^{-U(\mathbf{q})_i}\mathrm{d}\mathbf{q}}$, and $U(\mathbf{q})_i$ is the dimensionless energy of sample with coordinate vector $\mathbf{q}$ in state i. O_{ij} is recently proven by us to be related with the effective sample size and is bounded by 0.5 and $(2n)^{-1}$, with n being the sample size.[30] Therefore, accurate estimates of this scalar require sufficient samples, especially for transformations with small overlaps. For instance, for overlap as small as 0.01, we need at least 50 samples to reach the correct answer, and more samples are required for accurate and precise estimates. Therefore, it is important to check the value of this scalar.

Here we seek for the nonequilibrium generalization of the above equation in estimating the convergence in nonequilibrium pulling. The overlap scalar estimates the reliability of reweighting, even in nonequilibrium simulation. As is obviously shown in Eq. (11), the overlap scalar is not an explicit function of the energy difference $\Delta U(\mathbf{q})_{ij} = U(\mathbf{q})_i - U(\mathbf{q})_j$. Therefore, the scalar is not an explicit function of the nonequilibrium generalization of the energy difference, the nonequilibrium work W_{ij}. Thus we cannot estimate O_{ij} directly from the distribution of work in nonequilibrium simulation.

An alternative calculation method is from the variance of the free energy estimate or equivalently from the weight of each sample. As has been derived previously by Bennett,[68] the overlap scalar is nonlinearly dependent on the variance of BAR, namely

$$\sigma_{ij}^2 = \left(\int \frac{n_i n_j \rho_i \rho_j \mathrm{d}\mathbf{q}}{n_i \rho_i + n_i \rho_j} \right)^{-1} - \frac{1}{n_i} - \frac{1}{n_j} = \frac{1}{n}\left(\left(O_{ij} \right)^{-1} - 2 \right) \tag{12}$$

. Here the equal sample size rule of $n_i = n_j = n$ is applied. With the above equation, we can obtain the value of the overlap in nonequilibrium pulling from the variance of CE. As statistical convergence often requires the standard error to be smaller than some threshold, if we set the threshold as σ_{ref}, the number of samples needed to achieve the convergence level determined by the size of standard error depends negatively on the phase space overlap, namely

$$n = \frac{1}{\sigma_{ref}^2}\left(\left(O_{ij} \right)^{-1} - 2 \right) \tag{13}$$

. We note that small standard errors sometimes do not indicate well-converged results. The variance of the free energy is intrinsically more biased than the free energy itself.[30] Therefore, to determine the convergence, the time-evolution of various statistical quantities such as the free energy and its variance are also needed to be considered, as has been pointed out in our previous discussion.

Computational Details

System preparation. Our test structural observables include one periodic CV of the backbone dihedral and one non-periodic CV of the end-to-end distance of deca-alanine. For the dihedral case, instead of the simplest C_2H_6, we choose the caps in biomolecules, the ACE-NME system, which is more biologically relevant. For the distance case, the end-to-end distance is defined as the distance between the carbon atom of the carboxyl group of N-terminus and that of the C-terminus. The stretching of deca-alanine leads to the deformation of helical structures. The definitions of CVs along with the structures are given in Fig. S1. The value of alchemical CV can be the MM Hamiltonian described with AMBER 99SB[74] force filed and the semi-empirical QM Hamiltonian of PM3[75] and PM6.[76]

The dihedral system is solvated into TIP3P water molecules[77-78] in a rectangular box replicated in the whole space with periodic boundary conditions. The minimum distance between any atoms originally present in solute and the edge of the periodic box is set to be 10 Å and the number of triangulated 3-point water molecules is 511. The stretching of deca-alanine is performed in vacuo. The size of the QM region in each test system is given in Table 1.

MD simulation. The dihedral windows or segments are equally spaced from 0° to 360 ° with 2° increments and the large force constant of 1000 kcal/mol·rad^2 is used in nonequilibrium pulling and initial configuration sampling in order to define the initial state precisely. This large force constant ensures the precise definition of states in conformational space and the validity of the stiff string approximation. In each intermediate along the physically meaningful CV, we perform 2000 cycles energy-minimization with steepest descent algorithm. The system is gradually heated from 0 K to 300 K in an NVT ensemble over a period of 10 ps, after which 200 ps NPT equilibration is performed.

In the distance case, the distance windows are spaced equally from 13 Å to 23 Å with 0.5 Å increments and the force constant of 500 kcal/mol·Å^2 is used. The procedure of equilibration before the initial configuration sampling is the same with the dihedral case, namely 2000 cycles of minimization, 10 ps heating and 200 ps equilibration.

After equilibration, the initial configuration sampling is performed with the sampling interval of 0.05 ps in the dihedral case and the sampling interval of 0.1 ps in the distance case. The CVs are used as the observable to define statistical inefficiency to subsample independent configurations.[66] According to our autocorrelation analysis, these sampling intervals are similar to the typical autocorrelation time for these systems. The nonequilibrium trajectories are then initiated from these uncorrelated configurations. For convergence check, we tested a series of pulling speeds. For the dihedral case, we tested 0.5 ps per 2° segment, 1 ps/segment and 2 ps/segment. For the distance case, we tested 1000 Å/ns, 250 Å/ns and 50 Å/ns.

The simulations along the alchemical CV use the initial configurations sampled in the above simulations. Each perturbation of the alchemical control parameter is $\Delta\lambda = 0.02$ for ACE-NME and $\Delta\lambda = 0.001$ for deca-alanine. The relaxation time between successive perturbations is 1 fs. The PM3 and PM6 simulations are initiated from MM equilibrated configurations. All other settings are the same with the MM settings.

In the periodic simulation of the solvated dihedral case, a cutoff of 9 Å for non-bonded interactions in the real space is applied and long-range electrostatics are treated with PME method.[79] Isotropic position scaling along with Berendsen barostat is employed to regulate the pressure. In the vacuum simulation, no cutoff for non-bonded interactions is used.

In all simulations, the SHAKE[80] algorithm is applied to perform bond length constraints for bonds involving hydrogen atoms in all molecules.[81] The time step used is 1 fs. Langevin dynamics[82] with the collision frequency of 5

ps^{-1} are implemented for temperature regulation. MD simulations are performed with AMBER[83] suite and statistical analysis are obtained with homemade codes.

Result and discussion

1. Periodic CV and small system -- the backbone dihedral of ACE-NME.

Firstly, we check the convergence of all direct calculations of the free energy profiles at MM, PM3 and PM6 levels. As is shown in Fig. 2a, 2c and 2e, the PMFs do not vary with the pulling speed, which indicates the pulling speed of 0.5 ps/segment is slow enough for converged sampling. Therefore, we compare the results obtained from 0.5 ps per segment. The convergence of the PMF on the sample size is checked in Fig. 2b, 2d and 2f, from which we know the convergence of PMF is quite well. There are still some differences between the 20-sample PMF and the 25-sample PMF. Thus, we use the sample size of 25 to determine convergence in direct simulations. We should note that the point of minimal sample size for convergence here is very important in calculating the speedup of the indirect scheme. For this small system of ACE-NME, the absolute convergence can be reached with less than 5 ns sampling. If we overestimate the sample size needed for convergence in the direct QM/MM simulation, the speedup is also overestimated. For instance, in the case that the computational cost under MM Hamiltonian is much smaller than that under QM Hamiltonian, if the sample size required for convergence is 20 but we overestimate it to be 200, the indirect scheme leads to a further about 10 fold speedup, which exaggerates the performance and is erroneous.

The QM/MM correction terms are plotted as a function of CV in Fig. 3. The sample size dependence tells us that for MM<->PM3 and MM<->PM6 reweighting, 3 samples are already enough for convergence. However, we notice that the statistical noise in the correction terms is quite significant. Here we focus on the convergence determined by bias elimination. Namely, the PMF does not vary with the sample size. In this aspect, the convergence has been reached.

Then, we turn to combine the direct MM calculation with QM/MM corrections, which is given in Fig. 4. As the statistical noise in the QM/MM correction is quite large and the free energy profile is fluctuating significantly, we employ Savitzky-Golay filter to increase the signal-to-noise ratio and smooth the PMF. As we can see, the indirect scheme gives a similar profile with the direct one. The indirect QM/MM PMF agrees well with direct ones, but there are still some discrepancies. Although the difference between indirect and direct QM/MM results seems large, we note that this is due to the small increment on axis in our plot. The major spacing in Fig. 4b is 2 kcal/mol and the maximum of the absolute difference between indirect PM3 and direct PM3 in Fig. 4b is about 1 kcal/mol, which is much smaller than those reported in references. For instance, in one reference[54] the indirect QM/MM PMF differs from the direct result by 3 kcal/mol. In another reference the free energy of the transition state in an S_N2 reaction is underestimated by

6 kcal/mol.[50] Therefore, the accuracy our result is already acceptable. The PM6 curves behave similarly with the PM3 ones and thus are not re-discussed here.

As MM Hamiltonian differs from PM3 and PM6 relatively large, which does not satisfy our pursuit of perfect closure of thermodynamic cycle, to further validate the cycle closure of our indirect scheme and get a near perfect match, we then simulate the indirect PM6 scheme via reweighting from PM3 Hamiltonian. Direct PM3 calculation is performed and we compute PM3<->PM6 corrections and obtain indirect PM6 profile.

The resulted correction terms are checked for convergence in Fig. 5a. Again, we know that 3 samples are enough for PM3<->PM6 corrections. Then we combine them to get the PM6 PMF, as is shown in Fig. 5b and 5c. Now, a near perfect match can be seen. Both the raw indirect PM6 curve and the fitted indirect curve almost completely overlap with the direct PM6 curve. This phenomenon proves the correctness of our method. We note that this PM3<->PM6 calculation is only used for check the cycle closure in our thermodynamic cycle and practically leads to no computational speedup.

Then another question arises. Why MM<->QM/MM corrections introduce large errors? To answer this question, we check the standard deviation (SD) of each state. Their sum gives the statistical error of the whole PMF. Note that the SD of each state only indicates the contribution of samples from that state to the uncertainty of the free energy profile rather than the uncertainty of the free energy of that state, as the later one also correlates with the bias in the free energy profile. As the error in each state influence all other states, the statistical error may be the main source of error in the MM<->QM reweighting. Fig. 6a plots the SD of each state in the direct simulations under MM, PM3 and PM6 Hamiltonians. We notice that in the MM curve there are two peaks at about 90°and 270°. These regions are also the peaks in the MM PMF and correspond to the most unstable conformations under MM Hamiltonian. By contrast, PM3 and PM6 do not have this behavior and SDs from all states are of similar values. As a result, the free energy profiles at MM level suffer from statistical error, which is one of the main sources of error in the indirect scheme. Then we check the other component of the indirect scheme, the correction terms of MM<->PM3, MM<->PM6 and PM3<->PM6. As is shown in Fig. 6b, still, there are peaks in the SD profile of MM<->QM corrections, while there is no peak in the PM3<->PM6 curve. As a result, the combination of direct MM result and the MM<->QM corrections accumulates noises, leading to the non-perfect match between direct QM/MM result and the indirect PMF. Comparing Fig. 6a and Fig. 6b, we notice that the statistical error in transformation between different Hamiltonians is much larger than transformations under the same Hamiltonian. Thus, the correction terms contribute the most significant part of error in indirect QM/MM simulations.

Another observation in this correction comparison plot is that, with the same sample size, the statistical

errors in MM<->QM corrections are larger than the PM3<->PM6 ones, indicating the higher similarity between PM3 and PM6 Hamiltonians, compared with the similarities between MM and QM Hamiltonians. To quantify the similarities between different Hamiltonians, we calculate the overlap profile from the SD profile for MM<->PM6 and PM3<->PM6 corrections. In Fig. 7, there are wells in the overlap profile in MM<->PM6 corrections. We notice that these wells in the overlap profile and the peaks in the SD profile are at the same place. These wells (smaller overlaps) lead to higher errors and poorer convergence behavior. In PM3<->PM6 reweighting, the overlap scalar in each transformation is satisfactorily high and is higher than those in MM<->PM6 reweighting. Therefore, the selection of reference Hamiltonian used for sampling should be emphasized as a technical point in indirect QM/MM simulation. We summarized the SD profiles and overlap profiles in Fig. S2a and b, from which we notice that the direct simulation often has larger overlap and smaller SD and thus converge better, while the overlap for correction terms is relatively smaller and thus has larger statistical errors.

To check if this is triggered by the initial-configuration bias or the non-equilibrated effect in our simulation, we run extensive sampling at MM and PM3 level to check the time-dependence of state-specified SD. As is shown in Fig. 8, the two peaks in the MM curve are extremely hard to minimize, while the PM3 curve behaves well and all SDs are effectively minimized with further sampling. We notice that the dependence of SD on the sample size is nonlinear, which is expected according to Eq. (3).

Efficiency comparison between the direct and indirect scheme. The computational costs for the direct and indirect schemes are given in Table 2 and Table S1. We scale all the simulation times by the ratio of the computational cost of QM Hamiltonian to that of MM Hamiltonian to the equivalent simulation time under MM Hamiltonian, enabling direct comparison between their efficiencies. As can be seen, the indirect scheme does result in some saving of computational cost, compared with the direct QM/MM simulation. However, the small difference between computational cost under MM and QM Hamiltonian leads to small speedup ratio in the dihedral case. This is expected considering the scaling behavior of the computational cost of the QM/MM Hamiltonian on the system size. Also, considering the statistical noise introduced in the MM<->QM correction, we would recommend the direct QM/MM simulation rather than the indirect scheme, if small systems are under consideration.

2. Non-periodic CV and large system -- the end-to-end distance of deca-alanine.

The stretching of deca-alanine has been used as the test system for nonequilibrium enhanced sampling techniques in a number of researches.[5, 84-85] Therefore, it is the ideal system for us to test the performance of our multi-dimensional nonequilibrium free energy simulation scheme for indirect QM/MM simulation.

Firstly, we check the convergence behavior of direct calculations of PMF under different Hamiltonians. For this system, we only present direct and indirect PM6 results with MM Hamiltonian as intermediate, as the PM3 Hamiltonian behave similarly with PM6. The pulling speed dependence of the PMF is shown in Fig. 9a and 9c. The pulling speed of 250 Å/ns seems slow enough and the PMF under this speed is almost identical with the slowest speed of 50 Å/ns. Then we compare the PMFs under this speed (250 Å/ns) obtained from different sample sizes, which are given in Fig. 9b and 9d. The initial sample size is 5 and in each iteration further 5 samples are added to the dataset. From the MM plot of Fig. 9b, we know that the convergence at MM level can be achieved at about 25 samples. Smaller sample sizes still result in fluctuations in the PMF, although this fluctuation is rather small. The maximum difference between the fully converged PMF and PMFs in the first 5 iterations is about than k_BT (0.59 kcal/mol), not to say the root mean square deviation. As has been discussed in the previous example, the underestimate of the convergence sample size at low-level Hamiltonians and the overestimate of the convergence sample size at high-level Hamiltonians result in an overestimated speedup of the indirect scheme. Therefore, to avoid exaggerating the performance of the indirect scheme, we set the sample size required for convergence at MM level as 25 samples. The convergence at PM6 level seems harder compared with that at MM level. The PMF keeps varying with the sample size and at least 50 samples are required for convergence. The sample size dependence of SD profile is shown in Fig. 9e and 9f. For this system, we notice that there is no peak in the SD profile. Therefore, all states contribute almost equally to the statistical error in reweighting and the better convergence behavior should be obtained.

As the stretching of deca-alanine does not include strong interactions such as ion-ion interactions, the free energy does not vary and fluctuate significantly with the end-to-end distance. Therefore, for sampling efficiency considerations, we use 1 Å increments from 13 Å to 23 Å in MM<->PM6 correction. The sample size dependence of the QM/MM corrections is given in Fig. 10a, from which we know that the MM<->PM6 corrections converge with 5 samples. Statistical noises still exist in this case and the curve fitting procedure is needed to get a smooth PMF. The standard error in each state in MM<->PM6 correction and the corresponding overlap profile are given in Fig. 10b. Compared with the simple ACE-NME case, for this larger system, slower pulling speeds in the alchemical space are needed for convergence, due to the larger size of QM region (109 atoms > 12 atoms, as is shown in Table 1) and thus the larger difference between MM and QM Hamiltonians. We notice that the SD profile seems to be negatively correlated with the overlap profile, which is correct according to Eq. (12). The overlaps from state 20 Å to 22 Å are quite small and thus their results are of less reliability.

Combining the direct MM calculation with the QM/MM corrections leads to the indirect PMF, which is given in Fig. 11. The raw indirect PMF agrees with the direct PMF in regions from 13 Å to 19 Å, while the outer 20-22 Å region seems to deviate relatively large and the last 23 Å point agrees with the reference direct PMF again. This is due

to the small overlaps in the 20-22 Å region and the unreliability discussed above. Considering the slow-varying nature of MM PMF, the PM6 PMF should neither fluctuate significantly. To get a smooth PMF and take the magnitude of statistical error into consideration at the same time, here we perform polynomial fitting with the raw data points. We weight each point by the reciprocal of its statistical uncertainty in order to consider the effect of statistical errors. Here we note that the reciprocal of variance is positively correlated with the overlap, as is defined in Eq. (12). Therefore, our weighted fitting procedure actually takes the phase space overlap into consideration. As is discussed previously, the reweighting results from state 20 Å to 22 Å are less unreliable and thus are weighted less. The resulted fitted curve agrees well with the direct PM6 result. We can expect that for slower pulling speeds the phase space overlap would increase and the raw data would become better.

Efficiency comparison between the direct and indirect scheme. The computational costs for the direct and indirect schemes in the distance case are given in Table 3. We again scale all the simulation times by the computational cost ratio of QM to MM in order to obtain the equivalent simulation time under MM Hamiltonian. As can be seen in the table, for large systems described with QM Hamiltonian, the indirect scheme results in higher speedup, compared with the direct QM/MM simulation. The main reason for this speedup is the large difference between computational costs under MM and QM Hamiltonians. Therefore, the conclusion for large systems differs from the small system one. For computationally demanding systems in direct QM/MM simulation, indirect QM/MM method gives significant speedups and should be applied.

3. When $\sigma_{ij} = O_{ij}$.

Another interesting phenomenon can be seen in Fig. 10b is that the SD profile intersects the overlap profile at 14 Å. As the SD profile is not dimensionless but with the unit of kcal/mol, we recover the dimensionless SD profile of ACE-NME and deca-alanine systems in Fig. S2. From Fig. S2a and c, we notice that in direct MM and QM simulations the phase space overlap is very large and the state-specified SD is much smaller than the overlap scalar, while in MM<->QM corrections of Fig. S2b and d, the overlap is relatively small and its value is similar to the SD. This phenomenon is in agreement with the good convergence behavior of direct free energy simulations and the relatively poor convergence behavior of MM<->QM corrections. In Fig. S2d, the SD and overlap curves do not intersect at 14 Å and the SD curve is always higher than the overlap profile. According to the sample size dependence of σ_{ij} in Eq. (4), when the sample size becomes larger, the SD curve will intersect with the overlap profile and then become further smaller and lower than the overlap curve. This phenomenon inspires us of another interesting mathematical question: When will the standard error in bidirectional reweighting equals the overlap scalar? What does

this mean? Setting the condition of $\sigma_{ij} = O_{ij}$ in the Eq. (12) leads to the following cubic equation,

$$O_{ij}^3 + \frac{2}{n} O_{ij} - \frac{1}{n} = 0 \quad (14)$$

. We do some math and obtain one real root and two complex roots, with e.g. the Cardano's method. As the sample size is a real number, we focus on the real root of

$$O_{ij} = \sigma_{ij} = \sqrt[3]{\frac{1}{2n}\left(1+\sqrt{1+\frac{32}{27n}}\right)} + \sqrt[3]{\frac{1}{2n}\left(1-\sqrt{1+\frac{32}{27n}}\right)} \quad (15)$$

, where n denotes the sample size. The analytical result is plotted in Figure S3, from which we notice that when the phase space overlap becomes small, more samples are needed to achieve the above condition. Also, when the overlap is small, the sample size seems to vary linearly with the overlap in the log-log plot. This is expected as when the sample size becomes large or the overlap scalar is small, the term $\frac{32}{27nk^2} \ll 1$ and approximately $O_{ij} = \sigma_{ij} \approx \sqrt[3]{\frac{2}{2n}} = n^{-\frac{1}{3}}$. Namely, the sample size required for achieving the above equation is approximately proportional to O_{ij}^{-3}, when the overlap is small.

According to our previous derivation, the overlap scalar is always smaller than 0.5.[30] Therefore, when $O_{ij} = \sigma_{ij}$, the standard error must decrease to be smaller than $0.5\, k_B T$. Specifically, the threshold is smaller than $0.5\, k_B T$ and varies with the phase space overlap. For overlaps as small as 0.01, the threshold becomes $0.01\, k_B T$. Although the phase space overlap is small, such small statistical uncertainty normally indicates good convergence behavior. Therefore, this condition can be viewed as an extension of the variance or standard error criterion and is a tight version of it. As the threshold for the standard error to determine convergence is often case-dependent and it is difficult to define a general threshold, the current criterion can serve as an empirical criterion for convergence check. The direct simulations all satisfy the condition of $\sigma_{ij} < O_{ij}$. The above data of convergence behavior in different systems suggest the following empirical rule: a) when σ_{ij} is smaller than O_{ij}, the simulation is well-converged, b) when σ_{ij} and O_{ij} are of similar size, the convergence is acceptable, c) when σ_{ij} is much larger than O_{ij}, the convergence behavior is bad. In another study of the base flipping case in DNA duplex, the empirical criterion is also shown to be valid.[86]

4. Lesson learned from nonequilibrium indirect QM/MM simulations.

Now we discuss the limitation of indirect QM/MM simulations and experiences obtained in the current work.

Although the system size influences the speedup of the indirect scheme, the size of the system also correlates with the dissimilarity between MM and QM Hamiltonians, which results in small phase space overlaps and limits the speedup of the indirect scheme. Slower pulling speeds are required for transformations between significantly different Hamiltonians. This, again, emphasizes the importance of selecting appropriate low-level Hamiltonians to maximize the similarity between the low-level and high-level Hamiltonians and thus maximize the efficiency of the indirect scheme.

The magnitude of the speedup of indirect semi-empirical QM simulations via MM intermediates ranges from 2 to 35. We note that our test QM Hamiltonians only include semi-empirical QM methods, while for higher-level ab initio / DFT calculations,[87-89] the speedup should be even more dramatic. For instance, in references, the indirect ab initio calculation at higher QM levels via the equilibrium limit (i.e. instantaneous perturbation limit) of the current nonequilibrium indirect scheme, namely via single-step free energy perturbation or linear response approximation, is often more than one order of magnitude faster than the direct scheme.[51-52] Further, an emphasis on the rational determination of the sample size required for convergence in direct QM/MM simulation is reported. Overestimation of the minimal sample size for convergence exaggerates the speedup given by the indirect scheme. The phase space overlap needs to be checked in reweighting. When the phase space overlap between the low-level intermediates and the high-level target Hamiltonian is small, the staging method is required. This leads to a dramatic increase in the computational cost of the indirect scheme. The current nonequilibrium pulling scheme is the generalization of previously proposed equilibrium perturbation methods, and reliable convergence can always be achieved with slow enough pulling.

Conclusion

The construction of free energy landscapes at QM/MM level is computationally demanding. The indirect schemes for QM/MM free energy simulation speed up the calculation. In this work, we reported a multi-dimensional nonequilibrium enhanced sampling scheme for indirect QM/MM free energy simulation. The method is able to recover the free energy profile along the physically meaningful CV at QM level indirectly, by combining the direct MM free energy profile and the alchemical correction term between MM and QM descriptions. Only nonequilibrium transformations are performed in this method. This nonequilibrium scheme of indirect QM/MM free energy simulation method can be seen as the generalization of previously proposed equilibrium perturbation based indirect QM/MM simulation methods. The benchmark cases include one periodic dihedral and one non-periodic distance. The cycle closure is checked numerically and a near perfect match is obtained. Moreover, the statistical noise in the indirectly constructed QM/MM PMF is found to be rather significant. Thus, an additional curve fitting procedure (e.g.

the Savitzky-Golay filter) is useful to smooth the curve. Besides, the speedup of the indirect scheme is found to be positively correlated with the size of the system or the QM region. For the small systems the speedup is only about a factor of 2, while for large systems it can be as large as 35. Considering the statistical errors involved in the indirect simulations, the direct scheme renders more reliable, accurate and precise estimates of the free energy profile for small systems, while for large systems the indirect scheme is advisable to be employed to accelerate the free energy simulations.

Acknowledgement

This work was supported China Scholarship Council and National Key R&D Program of China (Grant no. 2016YFA0501700). Computer access to the CLAIX cluster of RWTH Aachen University and clusters of Forschungszentrum Juelich is gratefully acknowledged. We thank Prof. Dr. Paolo Carloni (Forschungszentrum Juelich) and Abhijit Kayal (Quantumzyme) for valuable comments and critical reading.

Conflicts of interest

There are no conflicts of interest to declare.

Supporting information

Structures of simulated systems, definitions of CVs and the comparison between the dimensionless SD profiles and overlap profiles are given.

References

1. Battimelli, G.; Ciccotti, G., Berni Alder and the pioneering times of molecular simulation. *The European Physical Journal H* **2018,** *43* (3), 303-335.
2. Gallavotti, G., Ergodicity: a historical perspective. Equilibrium and Nonequilibrium. *The European Physical Journal H* **2016,** *41* (3), 181-259.
3. Lebon, G.; Jou, D., Early history of extended irreversible thermodynamics (1953–1983): An exploration beyond local equilibrium and classical transport theory. *The European Physical Journal H* **2015,** *40* (2), 205-240.
4. Inaba, H., The development of ensemble theory. *The European Physical Journal H* **2015,** *40* (4-5), 489-526.
5. Echeverria, I.; Amzel, L. M., Helix propensities calculations for amino acids in alanine based peptides using Jarzynski's equality. *Proteins: Structure, Function, and Bioinformatics* **2010,** *78* (5), 1302-1310.
6. Lee, T. S.; Radak, B. K.; Huang, M.; Wong, K. Y.; York, D. M., Roadmaps through free energy landscapes calculated using the multi-dimensional vFEP approach. *J Chem Theory Comput* **2014,** *10* (1), 24-34.
7. Sun, Z.; Wang, X.; Zhang, J. Z. H., Protonation-dependent base flipping in the catalytic triad of a small RNA. *Chem. Phys. Lett.* **2017,** *684*.
8. Moraca, F.; Amato, J.; Ortuso, F.; Artese, A.; Pagano, B.; Novellino, E.; Alcaro, S.; Parrinello, M.; Limongelli, V., Ligand binding to telomeric G-quadruplex DNA investigated by funnel-metadynamics simulations. *Proc. Natl. Acad. Sci. U.S.A.* **2017,** *114* (11), E2136.
9. Bruckner, S.; Boresch, S., Efficiency of alchemical free energy simulations. II. Improvements for thermodynamic integration. *J. Comput. Chem.* **2011,** *32* (7), 1320–1333.
10. Resat, H.; Mezei, M., Studies on free energy calculations. I. Thermodynamic integration using a polynomial path. *J. Chem. Phys.* **1993,** *99* (8), 6052-6061.
11. Resat, H.; Mezei, M., Studies on free energy calculations. II. A theoretical approach to molecular solvation. *J. Chem. Phys.* **1994,** *101* (7), 6126-6140.
12. Paliwal, H.; Shirts, M. R., A Benchmark Test Set for Alchemical Free Energy Transformations and Its Use to Quantify Error in Common Free Energy Methods. *J Chem Theory Comput* **2011,** *7* (12), 4115-34.
13. Fenwick, M. K.; Escobedo, F. A., On the use of Bennett's acceptance ratio method in multi-canonical-type simulations. *J Chem Phys* **2004,** *120* (7), 3066-74.
14. Sun, Z. X.; Wang, X. H.; Zhang, J. Z. H., BAR-based optimum adaptive sampling regime for variance minimization in alchemical transformation. *Phys. Chem. Chem. Phys.* **2017,** *19* (23), 15005-15020.
15. Procacci, P.; Chelli, R., Statistical Mechanics of Ligand–Receptor Noncovalent Association, Revisited: Binding Site and Standard State Volumes in Modern Alchemical Theories. *J. Chem. Theory Comput.* **2017,** *13* (5), 1924-1933.
16. Wang, X.; Tu, X.; Zhang, J. Z. H.; Sun, Z., BAR-based optimum adaptive sampling regime for variance minimization in alchemical transformation: the nonequilibrium stratification. *Phys. Chem. Chem. Phys.* **2018,** *20* (3), 2009-2021.
17. Sun, Z.; Wang, X.; Song, J., Extensive Assessment of Various Computational Methods for Aspartate's pKa Shift. *J. Chem. Inf. Model.* **2017,** *57* (7), 1621-1639.
18. Zwanzig, R. W., High temperature equation of state by a perturbation method. *I.nonpolar Gases J.chem.phys* **1954,** *22* (8), 1420-1426.
19. Mezei, M., Adaptive umbrella sampling: Self-consistent determination of the non-Boltzmann bias. *J. Comput. Phys.* **1987,** *68* (1), 237-248.
20. Hooft, R. W.; van Eijck, B. P.; Kroon, J., An adaptive umbrella sampling procedure in conformational analysis using molecular dynamics and its application to glycol. *J. Chem. Phys.* **1992,** *97* (9), 6690-6694.
21. Kästner, J., Umbrella sampling. *Wiley Interdisciplinary Reviews: Computational Molecular Science* **2011,** *1* (6), 932-942.
22. Fukunishi, H.; Watanabe, O.; Takada, S., On the Hamiltonian replica exchange method for efficient sampling of biomolecular systems: Application to protein structure prediction. *J. Chem. Phys.* **2002,** *116* (116), 9058-9067.
23. Itoh, S. G.; Damjanovic, A.; Brooks, B. R., pH replica-exchange method based on discrete protonation states. *Proteins* **2011,** *79* (12), 3420-36.
24. Okur, A.; Wickstrom, L.; Layten, M.; Geney, R.; Song, K.; Hornak, V.; Simmerling, C., Improved Efficiency of Replica Exchange

Simulations through Use of a Hybrid Explicit/Implicit Solvation Model. *J. Chem. Theory Comput.* **2006,** *2* (2), 420.

25. Sabri, D. D.; Roitberg, A. E., Optimization of Umbrella Sampling Replica Exchange Molecular Dynamics by Replica Positioning. *J. Chem. Theory Comput.* **2013,** *9* (9), 4692–4699.

26. Sugita, Y.; Okamoto, Y., Replica-exchange molecular dynamics method for protein folding. *Chem. Phys. Lett.* **1999,** *314* (1-2), 141-151.

27. Sugita, Y.; Kitao, A.; Okamoto, Y., Multidimensional replica-exchange method for free-energy calculations. *J. Chem. Phys.* **2000,** *113* (15), 6042-6051.

28. Jarzynski, C., A nonequilibrium equality for free energy differences. *Phys. Rev. Lett.* **1997,** *78* (14), 2690-2693.

29. Mallick, K.; Moshe, M.; Orland, H., Supersymmetry and Nonequilibrium Work Relations. *Physics* **2008**.

30. Wang, X.; Sun, Z., A theoretical interpretation of variance-based convergence criteria in perturbation-based theories. *arXiv preprint arXiv:1803.03123* **2018**.

31. Wood, R. H.; Muhlbauer, W. C. F.; Thompson, P. T., Systematic errors in free energy perturbation calculations due to a finite sample of configuration space: sample-size hysteresis. *J. Phys. Chem.* **1991,** *95* (17), 6670-6675.

32. Gore, J.; Ritort, F.; Bustamante, C., Bias and error in estimates of equilibrium free-energy differences from nonequilibrium measurements. *Proc Natl Acad Sci U S A* **2003,** *100* (22), 12564-9.

33. Zuckerman, D. M.; Woolf, T. B., Theory of a systematic computational error in free energy differences. *Phys Rev Lett* **2002,** *89* (18), 180602.

34. Ballard, A. J.; Jarzynski, C., Replica exchange with nonequilibrium switches: enhancing equilibrium sampling by increasing replica overlap. *J. Chem. Phys.* **2012,** *136* (19), 194101.

35. Vaikuntanathan, S.; Jarzynski, C., Escorted free energy simulations: improving convergence by reducing dissipation. *Phys. Rev. Lett.* **2008,** *100* (19), 190601.

36. Dickson, A.; Dinner, A. R., Enhanced Sampling of Nonequilibrium Steady States. *Annual Review of Physical Chemistry* **2010,** *61* (1), 441-459.

37. Hudson, P. S.; Woodcock, H. L.; Boresch, S., Use of Nonequilibrium Work Methods to Compute Free Energy Differences Between Molecular Mechanical and Quantum Mechanical Representations of Molecular Systems. *J Phys Chem Lett* **2015,** *6* (23), 4850-6.

38. Sun, Z.; Zhu, T.; Wang, X.; Mei, Y.; Zhang, J. Z., Optimization of convergence criteria for fragmentation methods. *Chem. Phys. Lett.* **2017,** *687*, 163-170.

39. Liu, W.; Sakane, S.; And, R. H. W.; Doren, D. J., The Hydration Free Energy of Aqueous Na+ and Cl- at High Temperatures Predicted by ab Initio/Classical Free Energy Perturbation: 973 K with 0.535 g/cm3 and 573 K with 0.725 g/cm3. *J.phys.chem.a* **2002,** *106* (7), 1409-1418.

40. Olsson, M. A.; Söderhjelm, P.; Ryde, U., Converging ligand-binding free energies obtained with free-energy perturbations at the quantum mechanical level. *J. Comput. Chem.* **2016,** *37* (17).

41. Raghavachari, K.; Saha, A., Accurate composite and fragment-based quantum chemical models for large molecules. *Chem. Rev.* **2015,** *115* (12), 5643-5677.

42. Collins, M. A.; Bettens, R. P., Energy-based molecular fragmentation methods. *Chem. Rev.* **2015,** *115* (12), 5607-5642.

43. Sahu, N.; Gadre, S. R., Molecular tailoring approach: a route for ab initio treatment of large clusters. *Accounts of chemical research* **2014,** *47* (9), 2739-2747.

44. Kitaura, K.; Ikeo, E.; Asada, T.; Nakano, T.; Uebayasi, M., Fragment molecular orbital method: an approximate computational method for large molecules. *Chem. Phys. Lett.* **1999,** *313* (3-4), 701-706.

45. Gao, J.; Luque, F. J.; Orozco, M., Induced dipole moment and atomic charges based on average electrostatic potentials in aqueous solution. *J. Chem. Phys.* **1993,** *98* (4), 2975-2982.

46. †, V. L.; Warshel, A., Microscopic models for quantum mechanical calculations of chemical processes in solutions: LD/AMPAC and SCAAS/AMPAC calculations of solvation energies. *J. Comput. Chem.* **1992,** *13* (2), 199–213.

47. Wesolowski, T.; Warshel, A., Ab Initio Free Energy Perturbation Calculations of Solvation Free Energy Using the Frozen Density Functional Approach. *J. Phys. Chem.* **1994,** *98* (20), 5183-5187.

48. Gao, J.; Xia, X., A priori evaluation of aqueous polarization effects through Monte Carlo QM-MM simulations. *Science* **1992,**

258 (5082), 631-5.

49. Zheng, Y. J.; Merz, K. M., Mechanism of the human carbonic anhydrase II-catalyzed hydration of carbon dioxide. *J. Am. Chem. Soc.* **1992,** *114* (26).

50. Lameira, J. S.; Kupchencko, I.; Warshel, A., Enhancing Paradynamics for QM/MM Sampling of Enzymatic Reactions. *J. Phys. Chem. B* **2016,** *120* (9), 2155.

51. Plotnikov, N. V.; Warshel, A., Exploring, refining, and validating the paradynamics QM/MM sampling. *J. Phys. Chem. B* **2012,** *116* (34), 10342-10356.

52. Plotnikov, N.; Kamerlin, S. C. L.; Warshel, A., ParaDynamics: An Effective and Reliable Model for Ab Initio QM/MM Free Energy Calculations and Related Tasks. *J. Phys. Chem. B* **2011,** *115* (24), 7950-62.

53. Bentzien, J.; Muller, R. P.; Florián, J.; Warshel, A., Hybrid ab initio quantum mechanics/molecular mechanics calculations of free energy surfaces for enzymatic reactions: the nucleophilic attack in subtilisin. *The Journal of Physical Chemistry B* **1998,** *102* (12), 2293-2301.

54. Polyak, I.; Benighaus, T.; Boulanger, E.; Thiel, W., Quantum mechanics/molecular mechanics dual Hamiltonian free energy perturbation. *J. Chem. Phys.* **2013,** *139* (6), 578.

55. König, G.; Boresch, S., Non-Boltzmann sampling and Bennett's acceptance ratio method: How to profit from bending the rules. *J. Comput. Chem.* **2011,** *32* (6), 1082-90.

56. Heimdal, J.; Rydberg, P.; Ryde, U., Protonation of the proximal histidine ligand in heme peroxidases. *J. Phys. Chem. B* **2008,** *112* (8), 2501-10.

57. Mikulskis, P.; Cioloboc, D.; Andrejić, M.; Khare, S.; Brorsson, J.; Genheden, S.; Mata, R. A.; Söderhjelm, P.; Ryde, U., Free-energy perturbation and quantum mechanical study of SAMPL4 octa-acid host-guest binding energies. *J. Comput. Aided Mol. Des.* **2014,** *28* (4), 375-400.

58. Fox, S. J.; Pittock, C.; Tautermann, C. S.; Fox, T.; Christ, C.; Malcolm, N. O.; Essex, J. W.; Skylaris, C. K., Free energies of binding from large-scale first-principles quantum mechanical calculations: application to ligand hydration energies. *J. Phys. Chem. B* **2013,** *117* (32), 9478-85.

59. Genheden, S.; Ryde, U.; Söderhjelm, P., Binding affinities by alchemical perturbation using QM/MM with a large QM system and polarizable MM model. *J. Comput. Chem.* **2015**.

60. Genheden, S.; Martinez, A. I. C.; Criddle, M. P.; Essex, J. W., Extensive all-atom Monte Carlo sampling and QM/MM corrections in the SAMPL4 hydration free energy challenge. *J. Comput. Aided Mol. Des.* **2014,** *28* (3), 187-200.

61. Fox, S. J.; Pittock, C.; Tautermann, C. S.; Fox, T.; Christ, C.; Malcolm, N. O. J.; Essex, J. W.; Skylaris, C. K., Free Energies of Binding from Large-Scale First-Principles Quantum Mechanical Calculations: Application to Ligand Hydration Energies. *J. Phys. Chem. B* **2013,** *117* (32), 9478-85.

62. Woods, C. J.; Manby, F. R.; Mulholland, A. J., An efficient method for the calculation of quantum mechanics/molecular mechanics free energies. *J. Chem. Phys.* **2008,** *128* (1), 152-159.

63. Caveayland, C.; Skylaris, C. K.; Essex, J. W., Direct Validation of the Single Step Classical to Quantum Free Energy Perturbation. *J. Phys. Chem. B* **2014,** *119* (3), 1017-25.

64. König, G.; Hudson, P. S.; Boresch, S.; Woodcock, H. L., MultiscaleFree Energy Simulations: An Efficient Methodfor Connecting Classical MD Simulations to QM or QM/MM Free EnergiesUsing Non-Boltzmann Bennett Reweighting Schemes. *J. Chem. Theory Comput.* **2014,** *10* (4), 1406-1419.

65. Rod, T. H.; Ryde, U., Quantum mechanical free energy barrier for an enzymatic reaction. *Phys. Rev. Lett.* **2005,** *94* (13).

66. Klimovich, P. V.; Shirts, M. R.; Mobley, D. L., Guidelines for the analysis of free energy calculations. *J. Comput. Aided Mol. Des.* **2015,** *29* (5), 397-411.

67. Shirts, M. R.; Bair, E.; Hooker, G.; Pande, V. S., Equilibrium free energies from nonequilibrium measurements using maximum-likelihood methods. *Phys Rev Lett* **2003,** *91* (14), 140601.

68. Bennett, C. H., Efficient estimation of free energy differences from Monte Carlo data. *J. Comput. Phys.* **1976,** *22* (2), 245-268.

69. Wang, X.; Xingzhao, T.; Boming, D.; John Z. H., Z.; Sun, Z., BAR-based Optimum Adaptive Steered MD for Configurational Sampling. *J. Comput. Chem.* **2019**.

70. Hummer, G.; Szabo, A., From the Cover: Free energy reconstruction from nonequilibrium single-molecule pulling experiments. *Proceedings of the National Academy of Science* **2001,** *98* (7), 3658-3661.
71. Hummer, G.; Szabo, A., Free energy reconstruction from nonequilibrium single-molecule pulling experiments. *Proceedings of the National Academy of Sciences* **2001,** *98* (7), 3658-3661.
72. Hummer, G.; Szabo, A., Free energy surfaces from single-molecule force spectroscopy. *Cheminform* **2005,** *36* (39), 504-13.
73. Paramore, S.; Ayton, G. S.; Voth, G. A., Extending the fluctuation theorem to describe reaction coordinates. *J. Chem. Phys.* **2007,** *126* (5), 992-992.
74. Hornak, V.; Abel, R.; Okur, A.; Strockbine, B.; Roitberg, A.; Simmerling, C., Comparison of multiple Amber force fields and development of improved protein backbone parameters. *Proteins* **2006,** *65* (3), 712-25.
75. Stewart, J. J., Optimization of parameters for semiempirical methods II. Applications. *J. Comput. Chem.* **1989,** *10* (2), 221-264.
76. Stewart, J. J., Optimization of parameters for semiempirical methods V: modification of NDDO approximations and application to 70 elements. *J. Mol. Model.* **2007,** *13* (12), 1173-1213.
77. Jorgensen, W. L.; Chandrasekhar, J.; Madura, J. D.; Impey, R. W.; Klein, M. L., Comparison of Simple Potential Functions for Simulating Liquid Water. *J. Chem. Phys.* **1983,** *79* (2), 926-935.
78. Price, D. J., A modified TIP3P water potential for simulation with Ewald summation. *J. Chem. Phys.* **2004,** *121* (20), 10096-103.
79. York, D. M.; Darden, T. A.; Pedersen, L. G., The effect of long‐range electrostatic interactions in simulations of macromolecular crystals: A comparison of the Ewald and truncated list methods. *J. Chem. Phys.* **1993,** *99* (10), 8345-8348.
80. Ryckaert, J. P.; Ciccotti, G.; Berendsen, H. J. C., Numerical integration of the cartesian equations of motion of a system with constraints: molecular dynamics of n -alkanes. *J. Comput. Phys.* **1977,** *23* (3), 327-341.
81. Miyamoto, S.; Kollman, P. A., Settle: An analytical version of the SHAKE and RATTLE algorithm for rigid water models. *J. Comput. Chem.* **1992,** *13* (8), 952-962.
82. Pastor, R. W.; Brooks, B. R.; Szabo, A., An analysis of the accuracy of Langevin and molecular dynamics algorithms. *Mol. Phys.* **1988,** *65* (6), 1409-1419.
83. Case, D. A.; Cheatham, T. E.; Tom, D.; Holger, G.; Luo, R.; Merz, K. M.; Alexey, O.; Carlos, S.; Bing, W.; Woods, R. J., The Amber biomolecular simulation programs. *J. Comput. Chem.* **2005,** *26* (16), 1668-88.
84. Park, S.; Khalili-Araghi, F.; Tajkhorshid, E.; Schulten, K., Free energy calculation from steered molecular dynamics simulations using Jarzynski's equality. *J. Chem. Phys.* **2003,** *119* (6), 3559-3566.
85. Ozer, G.; Quirk, S.; Hernandez, R., Adaptive steered molecular dynamics: Validation of the selection criterion and benchmarking energetics in vacuum. *J. Chem. Phys.* **2012,** *136* (21), 215104.
86. Wang, X.; Sun, Z., Determination of Base Flipping Free Energy Landscapes from Nonequilibrium Stratification. *DOI: 10.26434/chemrxiv.7376081* **2018**.
87. Zhao, Y.; Truhlar, D. G., The M06 suite of density functionals for main group thermochemistry, thermochemical kinetics, noncovalent interactions, excited states, and transition elements: two new functionals and systematic testing of four M06-class functionals and 12 other functiona. *Theor. Chem. Acc.* **2008,** *120* (1-3), 215-241.
88. Hertwig, R. H.; Koch, W., On the parameterization of the local correlation functional. What is Becke-3-LYP? *Chem. Phys. Lett.* **1997,** *268* (5), 345-351.
89. Chai, J. D.; Head-Gordon, M., Systematic Optimization of Long-Range Corrected Hybrid Density Functionals. *J. Chem. Phys.* **2008,** *128* (8), 57-63.

Table 1. The sizes of QM region and computational costs under MM and QM Hamiltonians for the dihedral case of solvated ACE-NME and the distance case of the stretching of deca-alanine in vacuo. The speed information reported is obtained with single-core simulation with restraints on the reaction coordinate. The speedup is the ratio of speeds under MM and QM Hamiltonians. The CPU used is Intel(R) Xeon(R) CPU E5-2695 v4 @ 2.10GHz.

Systems / Terms	ACE-NME			Deca-alanine		
	MM	PM6	PM3	MM	PM6	PM3
size of QM region		12 atoms			109 atoms	
speed(ns/day)	7.21	2.76	2.75	264.4	0.102	0.095
speedup(MM/QM)	1.00	2.61	2.62	1.000	2604.9	2783.2

Table 2. Efficiency comparison of direct and indirect QM/MM simulation for the dihedral case. Total simulation time in direct scheme is given by $N_{\text{segments}} * N_{\text{traj}} * (\phi_{\text{NEW}} + \phi_{\text{eq}})$, while the total simulation time in the indirect scheme is the sum of $N_{\text{segments,MM}} * N_{\text{traj.MM}} * (\phi_{\text{NEW,MM}} + \phi_{\text{eq,MM}})$ at MM level and $N_{\text{traj,MM->QM}} * (\phi_{\text{NEW,MM->QM}} + \phi_{\text{eq,MM}}) + N_{\text{traj,QM->MM}} * (\phi_{\text{NEW,QM->MM}} + \phi_{\text{eq,QM}})$ in MM<->QM correction. N_{segments} is the number of segments and N_{traj} is the number of realizations per segment. The simulation time at QM level is scaled by the ratio of computational cost under QM Hamiltonian and that under MM Hamiltonian in Table 1 to be the effective simulation time at MM level, enabling direct comparison between computational costs. The computational cost of MM->PM6 differs from PM6->MM, as the initial configuration sampling procedures proceed under different Hamiltonians. The PM3 result is similar and is given in Table S1.

Terms / Hamiltonian	ϕ_{eq} for each initial configuration (ps)	ϕ_{NEW} in each segment (ps)	Number of segments	Number of realizations per segment	Total simulation time (ps) scaled to MM Hamiltonian	Relative efficiency
direct MM	0.05	0.5x2=1	180	25	4725.00	2.61
MM->PM6	same with MM	0.05	same with MM	3	97.53	-
PM6->MM	same with PM6	0.05	same with MM	3	141.07	-
indirect PM6	-	-	-	-	4963.60	2.49
direct PM6	0.05	0.5x2=1	180	25	12343.21	1.00

Table 3. Efficiency comparison of direct and indirect QM/MM simulation for the distance case. Total simulation time in direct scheme is given by $N_{\text{segments}} * N_{\text{traj}} * (\phi_{\text{NEW}} + \phi_{\text{eq}})$, while the total simulation time in the indirect scheme is the sum of $N_{\text{segments,MM}} * N_{\text{traj.MM}} * (\phi_{\text{NEW,MM}} + \phi_{\text{eq,MM}})$ at MM level and $N_{\text{traj,MM->QM}} * (\phi_{\text{NEW,MM->QM}} + \phi_{\text{eq,MM}}) + N_{\text{traj,QM->MM}} * (\phi_{\text{NEW,QM->MM}} + \phi_{\text{eq,QM}})$ in MM<->QM correction. N_{segments} is the number of segments and N_{traj} is the number of realizations per segment. The simulation time at QM level is scaled by the ratio of computational cost under QM Hamiltonian and that under MM Hamiltonian in Table 1 to be the effective simulation time at MM level, enabling direct comparison between computational costs.

Terms / Hamiltonian	ϕ_{eq} for each initial configuration (ps)	ϕ_{NEW} in each segment (ps)	Number of segments	Number of realizations per segment	Total simulation time (ps) scaled to MM Hamiltonian	Relative efficiency
direct MM	0.1	2x2=4	20	25	2050.00	5209.85
MM->PM6	same with MM	1	11	5	143276.44	-
PM6->MM	same with PM6	1	11	5	157598.03	-
indirect PM6	-	-	-	-	302924.47	35.26
direct PM6	0.1	2x2=4	20	50	10680197.04	1.00

Fig. 1. a) An illustration of indirect QM/MM free energy simulation. Full MM transformation is performed and QM/MM corrections are performed at end states. b) An illustration of multi-dimensional free energy calculation. As we define k_1 as the configurational CV, k_2 as the alchemical CV, $K_2 = 1$ as the MM state and $K_2 = 2$ as the QM state, the direct QM/MM free energy simulation is the transformation from (1,K2=2) to (K1,K2=2) and the indirect scheme is the combination of the MM transformation (1,1) <-> (K1,1) and MM<->QM correction (k_1,1) <-> (k_1,2).

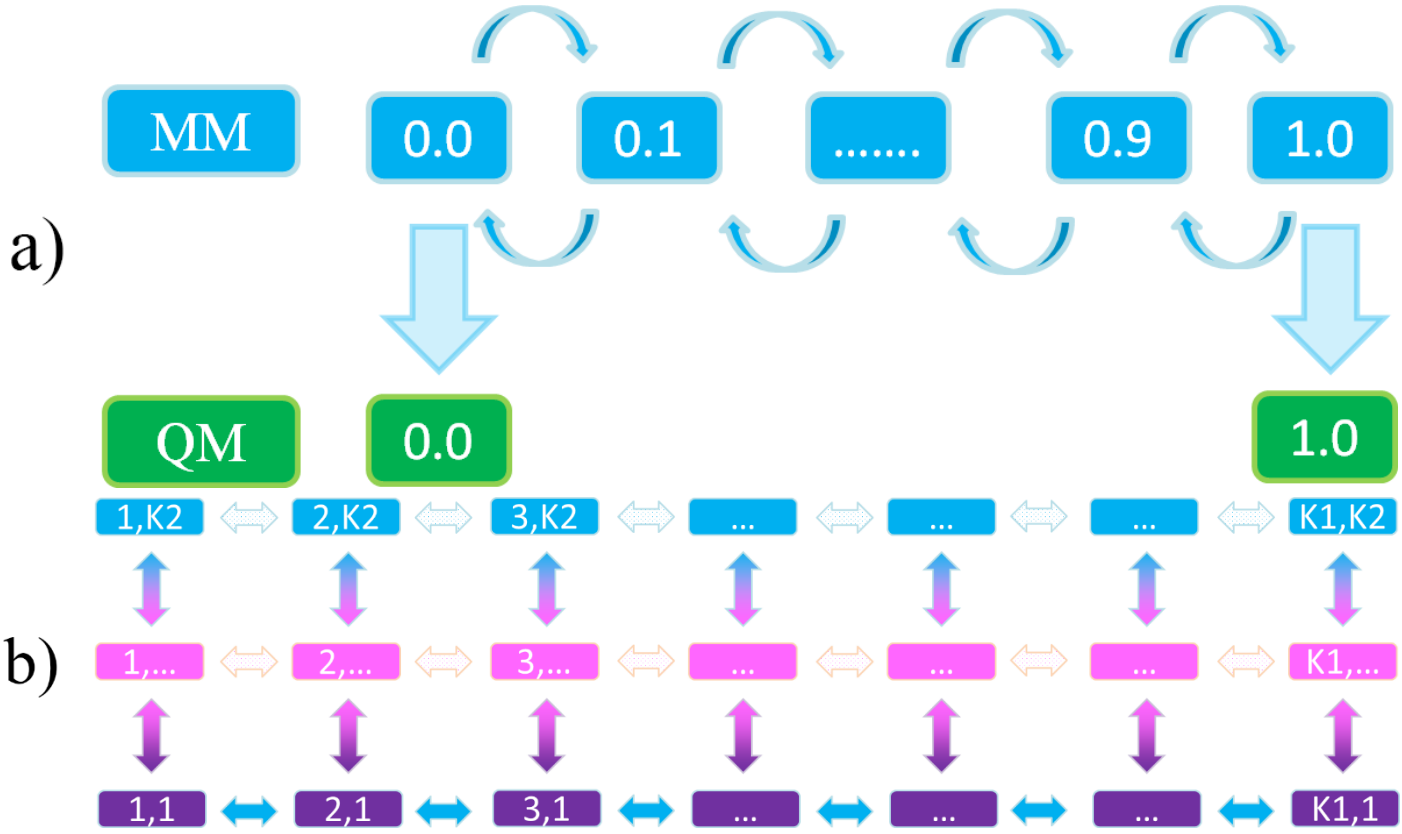

Fig. 2. In the dihedral case of ACE-NME, the convergence behavior of free energy profiles on the sample size and pulling speeds at a-b) MM, c-d) PM3 and e-f) PM6 levels. The initial sample size is 20 and in each iteration further 5 samples are added to the dataset. The legend x ps represents the pulling time for each 2° segment. We notice that 0.5 ps per segment is slow enough for absolute convergence and thus the statistics under this pulling speed is used for discussion in the following parts of the paper. There is small differences between the result obtained from the initial sample size and the that in the 2nd iteration. Therefore, we use the sample size 25 as the sample size for convergence.

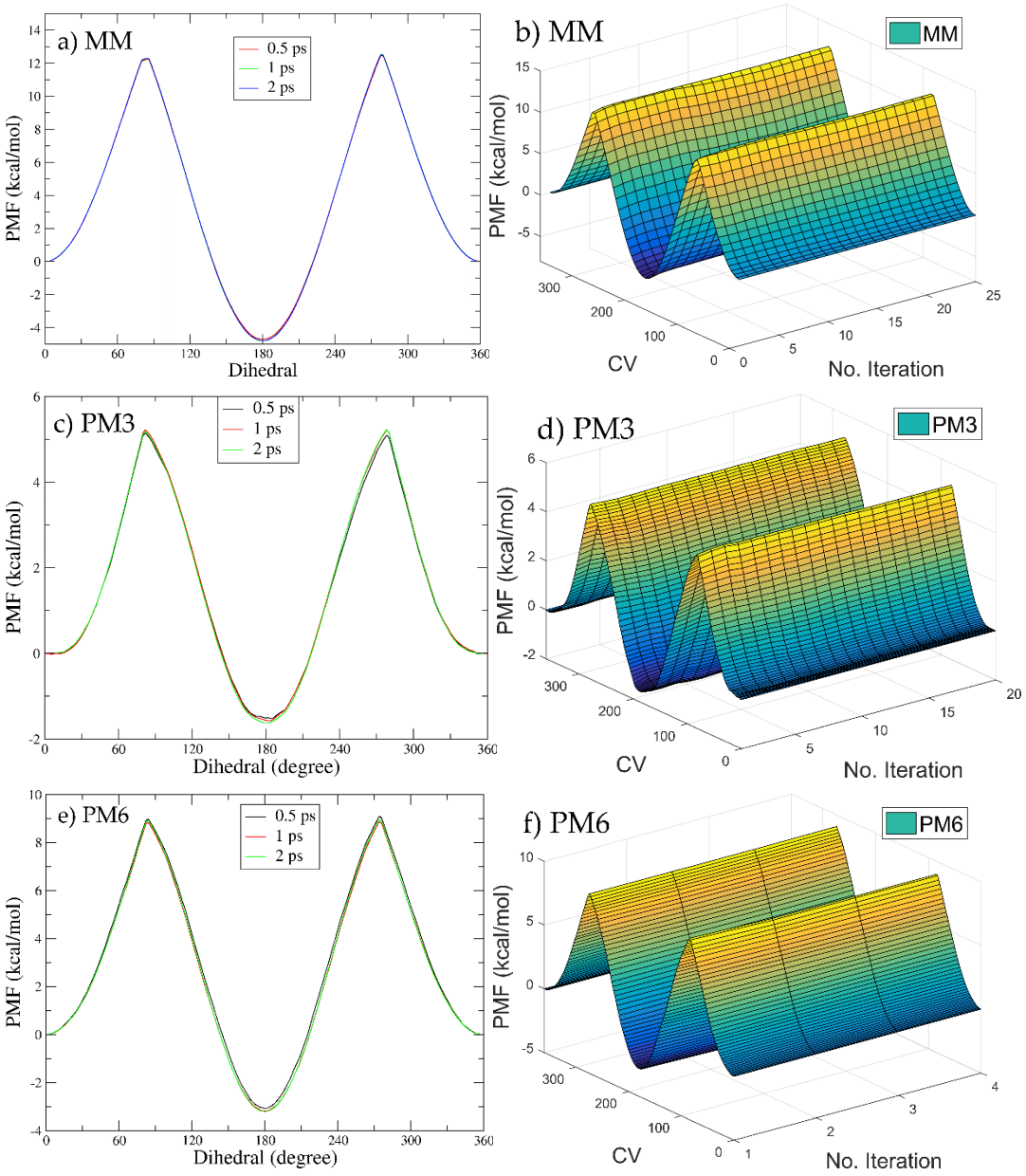

Fig. 3. Convergence of QM/MM correction PMF on the sample size in the dihedral ACE-NME case. a) MM<->PM3, b) MM<->PM6.

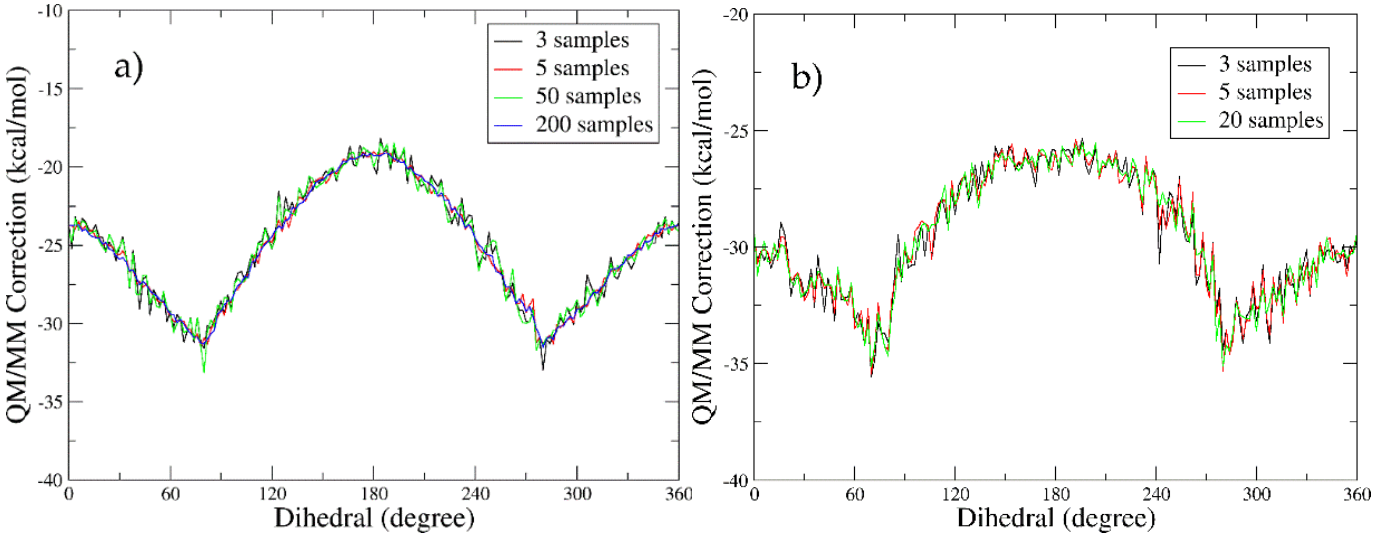

Fig. 4. Comparison between direct QM/MM PMF and indirect QM/MM PMF in the dihedral case. a) PM3 from MM and PM3/MM correction with error bars, b) smoothed PMF for PM3 from MM and PM3/MM correction, c) PM6 from MM and PM6/MM correction with error bars, d) smoothed PMF for PM6 from MM and PM6/MM correction. The error of curve fitting also depends on parameters and bias is also introduced. Error propagation is unable to quantitatively reflect the exact error or uncertainty. Thus the error bar of fitted curve is not given.

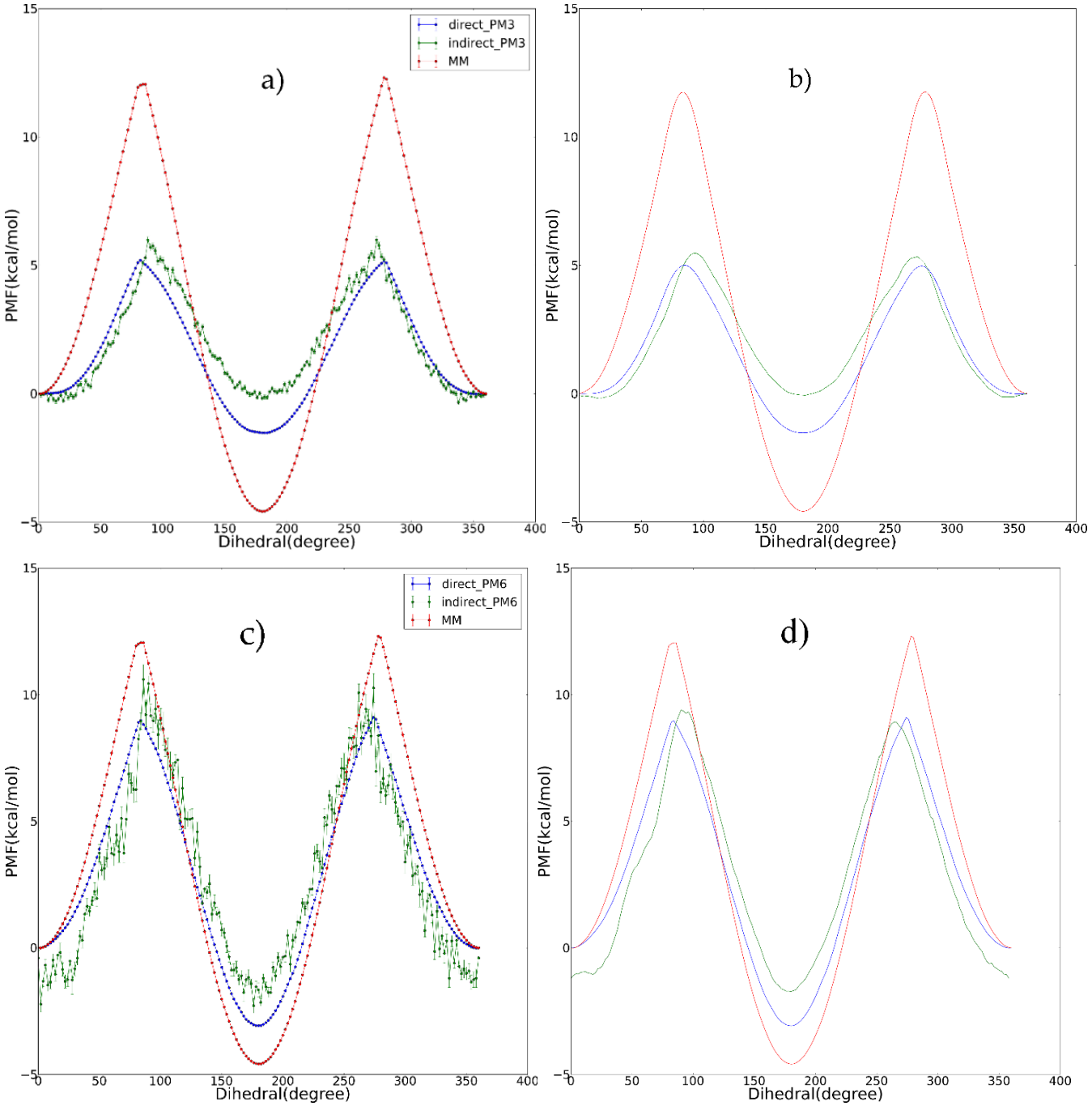

Fig. 5. Indirect QM/MM result obtained from reweighting from PM3 to PM6. a) Convergence of PM3<->PM6 correction PMF on the sample size. b-c) Comparison between direct QM/MM PMF and indirect QM/MM PMF. Here the PM6 result is obtained indirectly from PM3 PMF. b) The PM6 PMF from PM3 and PM3<->PM6 correction with error bars, c) smoothed PMF for PM6 from PM3 and PM3<->PM6 correction.

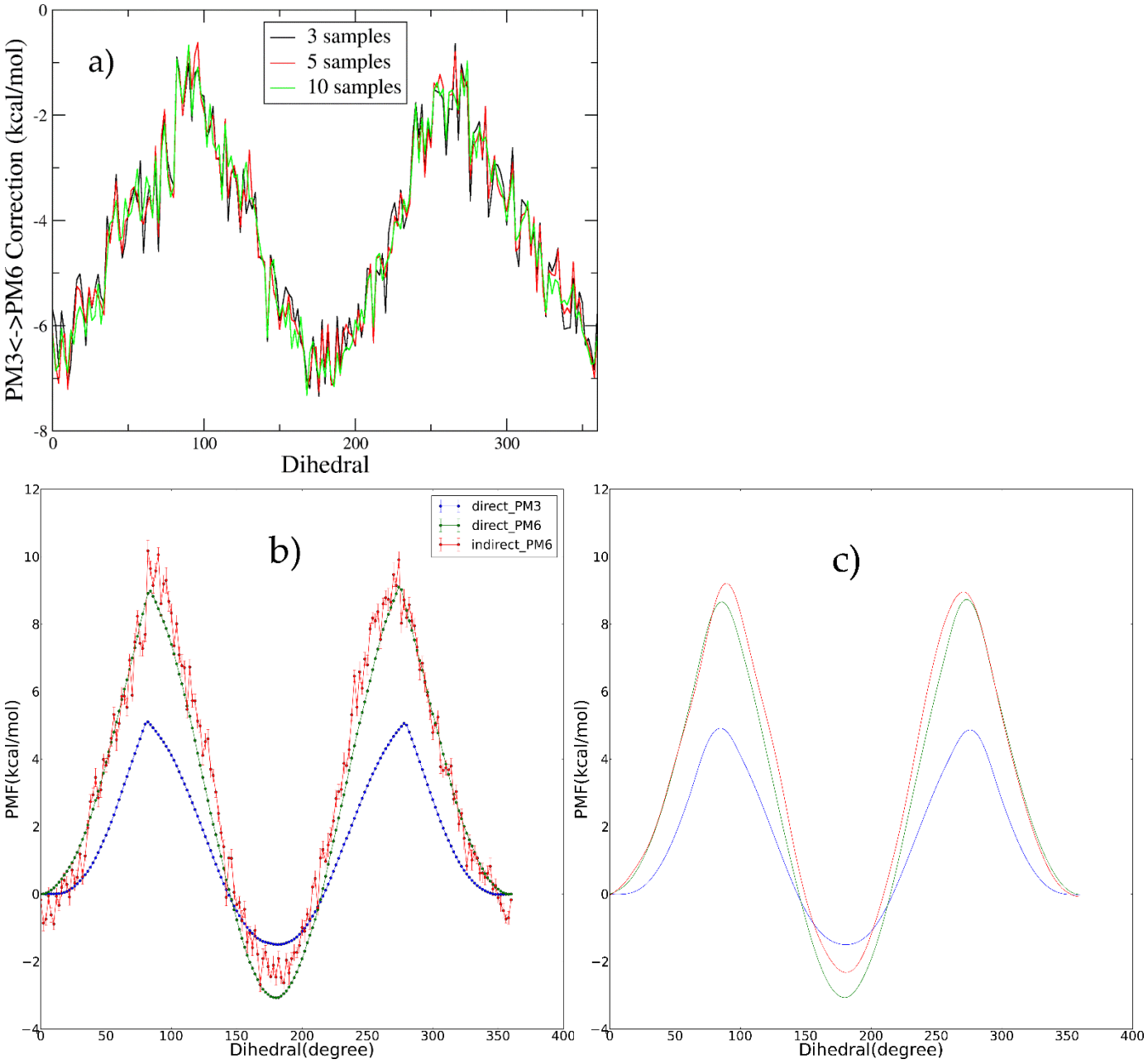

Fig. 6. a) State-specified SD with the same sample size (20 samples from each state) in the direct simulation under different Hamiltonians. We notice that even with the same sample size, the standard deviation under MM Hamiltonian has peaks around 90°and 270°, corresponding to the peaks in the PMF. This arises from the nature of the MM force field, leading to larger statistical noises around the peaks. The standard deviations contributed for samples from states under PM3 and PM6 are similar and do not have the peak-behavior under MM Hamiltonian. Therefore, better convergence between them can be achieved. b) Comparison of state-specified SD with the same sample size in MM<->PM3, MM<->PM6 and PM3<->PM6 corrections. These curves show similar behaviors of the SD profile in the direct simulation ones. Therefore, when the direct MM result is combined with the MM<->QM correction, the peak-behavior is further exaggerated and the states near the peaks in the SD profile accumulate statistically significant noises in the indirect simulation. We also notice that the error in PM3<->PM6 correction is smaller than corrections from MM to QM, which is consistent with the higher similarity between PM3 and PM6 than those between MM and QM Hamiltonians.

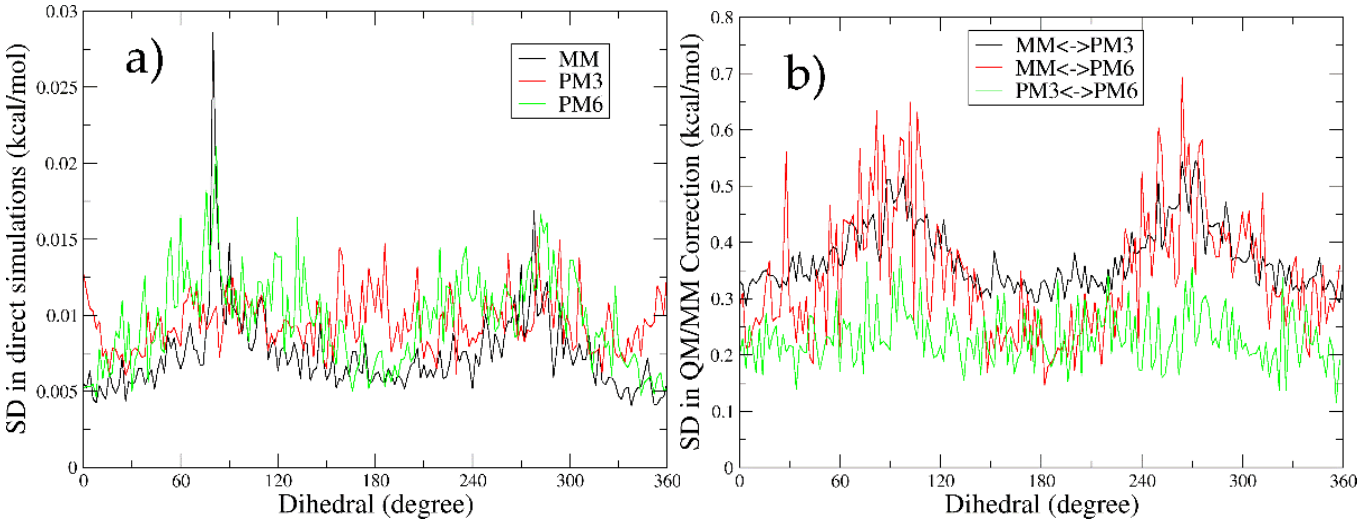

Fig. 7. Comparison of overlap scalars for MM<->PM6 and PM3<->PM6 corrections. The peaks in SD profile lead to the wells in the overlap scalar profile.

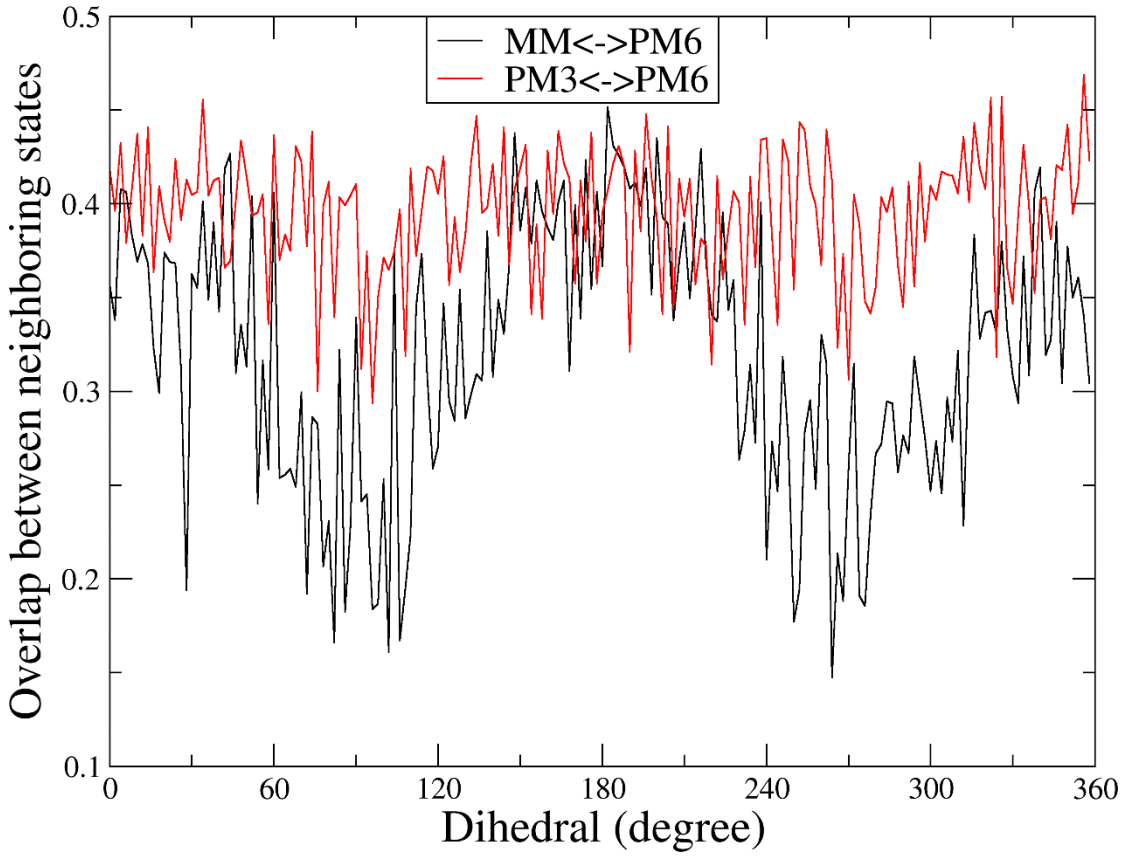

Fig. 8. Time-evolution of state-specified SD under MM and PM3 Hamiltonians. The initial sample size is 20 and in each iteration further 5 samples are added to the dataset. We notice that only the peaks of SD at MM level is extremely hard to decrease, while at PM3 level the SDs at all states behave similarly.

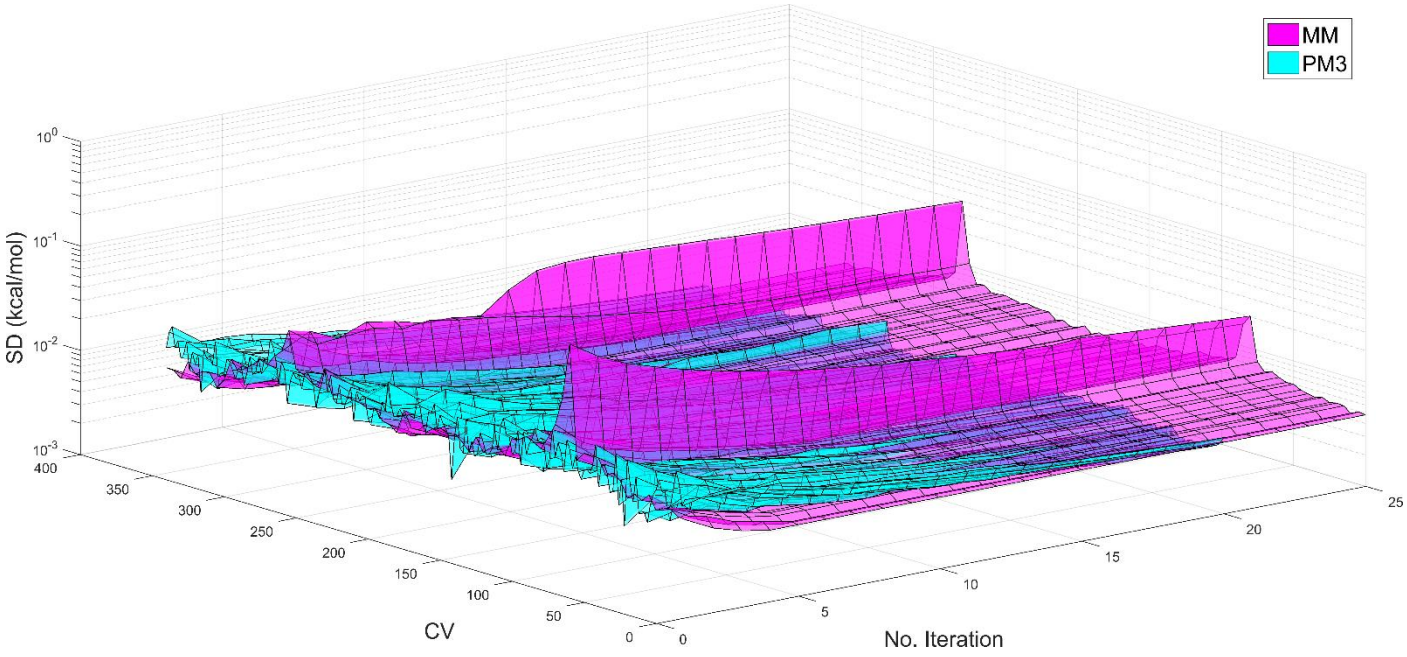

Fig. 9. In the distance case of deca-alanine, the convergence behavior of free energy profiles on the sample size and pulling speeds at a-b) MM, and c-d) PM6 levels. The initial sample size is 5 and in each iteration further 5 samples are added to the dataset. We notice that about 25 samples are needed to get the fully converged PMF at MM level while 50 samples are required for convergence at PM6 level. The PMF comparison under different pulling speeds uses fully converged PMFs. e) 2D plot for direct comparison between the SD profiles at MM and PM6 level. f) The time-evolution of state-specified SD at MM and PM6 levels. We notice that there is no peak in the SD profile.

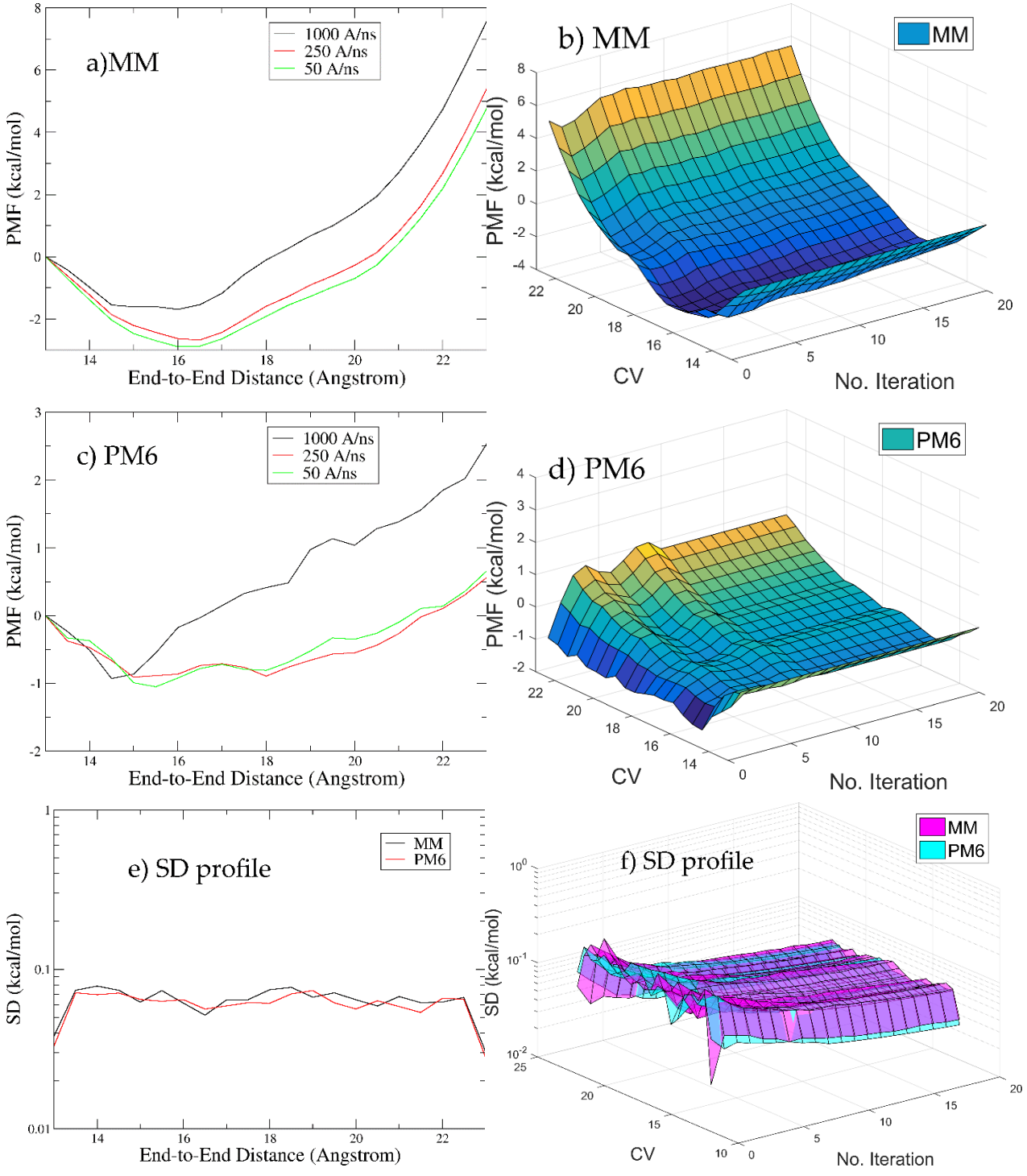

Fig. 10. a) Convergence of MM<->PM6 correction PMF on the sample size in the distance deca-alanine case. We notice that the correction term converged with about 5 samples. b) State-specified standard errors in MM<->PM6 corrections and the overlap profile in MM<->PM6 correction. The unit of SD is kcal/mol and the overlap scalar is dimensionless. Here we use the result obtained with 50 samples.

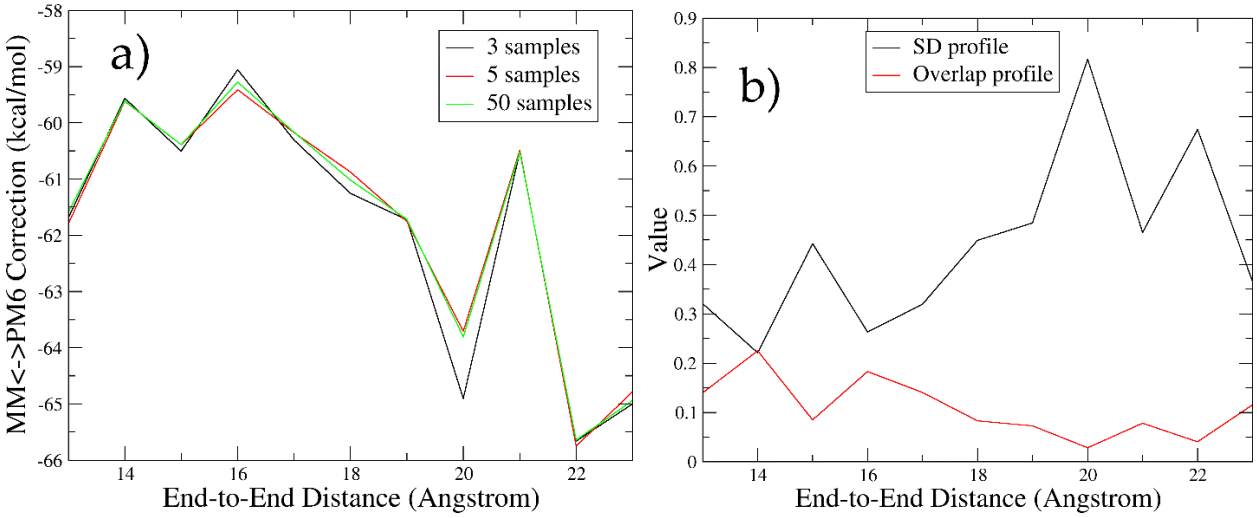

Fig. 11. Comparison between direct QM/MM PMF and indirect QM/MM PMF in the distance case. The QM level is PM6. Polynomial fitting is employed to smooth the PMF. The reciprocal of the variance of each data point is used to assign weights in the weighted fitting.

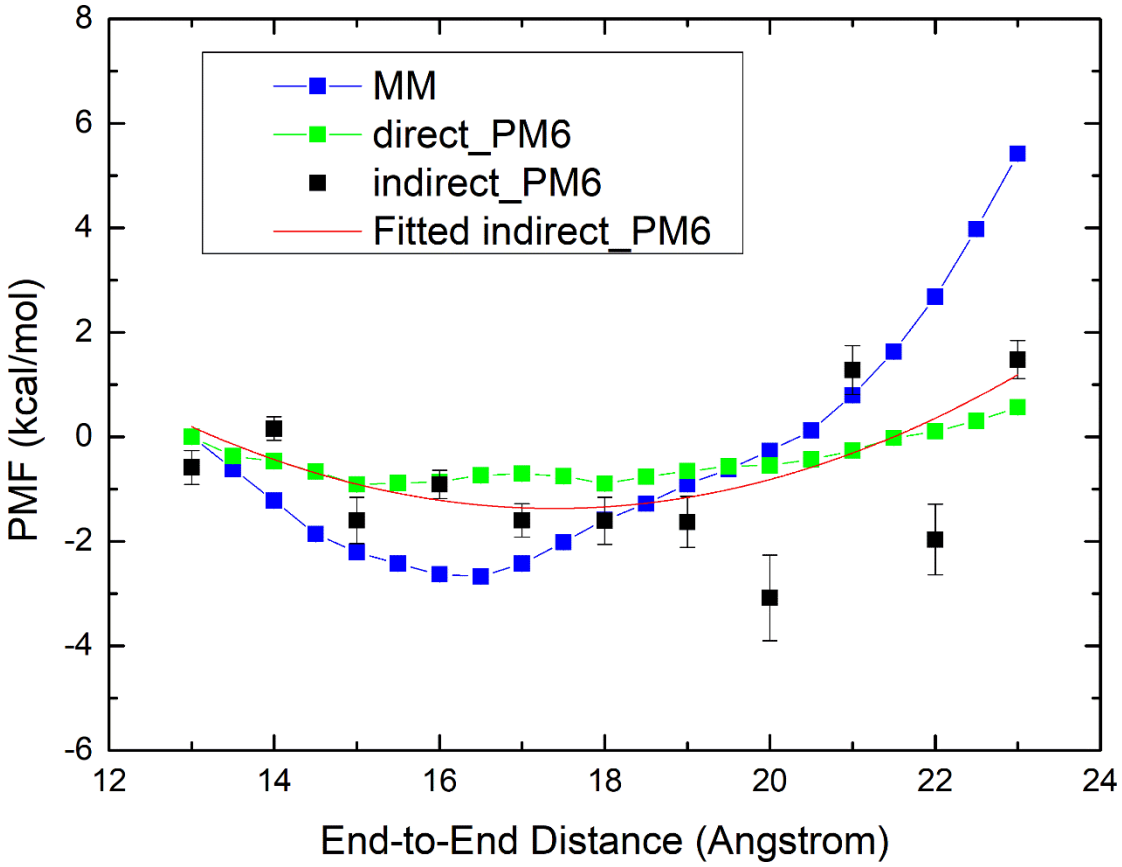

Supporting Information: BAR-based Multi-dimensional Nonequilibrium Pulling for Indirect Construction of QM/MM Free Energy Landscape

Xiaohui Wang[1,2], Qiaole He[3,4], and Zhaoxi Sun[1,3*]

[1]*State Key Laboratory of Precision Spectroscopy, School of Chemistry and Molecular Engineering, East China Normal University, Shanghai 200062, China*

[2]*Institute of Computational Science, Università della Svizzera italiana (USI), Via Giuseppe Buffi 13, CH-6900, Lugano, Ticino, Switzerland*

[3]*Computational Biomedicine (IAS-5/INM-9), Forschungszentrum Jülich, Jülich 52425, Germany, and Forschungszentrum Jülich GmbH, IBG-1: Biotechnology, Wilhelm-Johnen-Str. 1, 52425 Jülich, Germany*

[4]*State Key Laboratory of Bioreactor Engineering, R&D Center of Separation and Extraction Technology in Fermentation Industry, East China University of Science and Technology, Shanghai 200237, China*

*To whom correspondence should be addressed: proszx@163.com

Fig. S1. Definitions of reaction coordinates.(Red O atom, cyan C, white H, green Cl, blue N atom.). a) the backbone dihedral in ACE-NME (C-C-N-C).

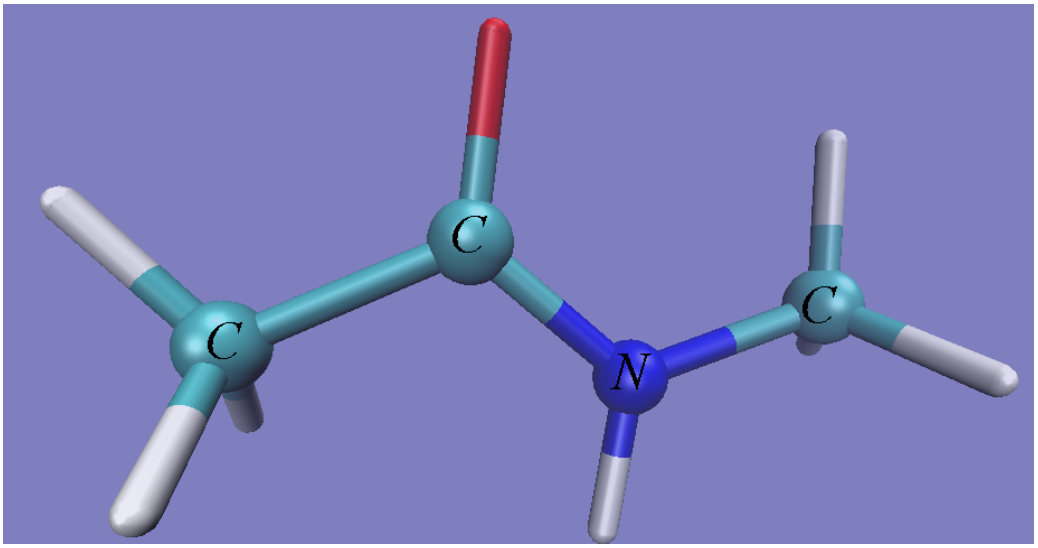

b) The end-to-end distance defined as the distance between carbon atom of the carboxyl group of N-terminus and that of the C-terminus is used to describe the stretching of deca-alanine.

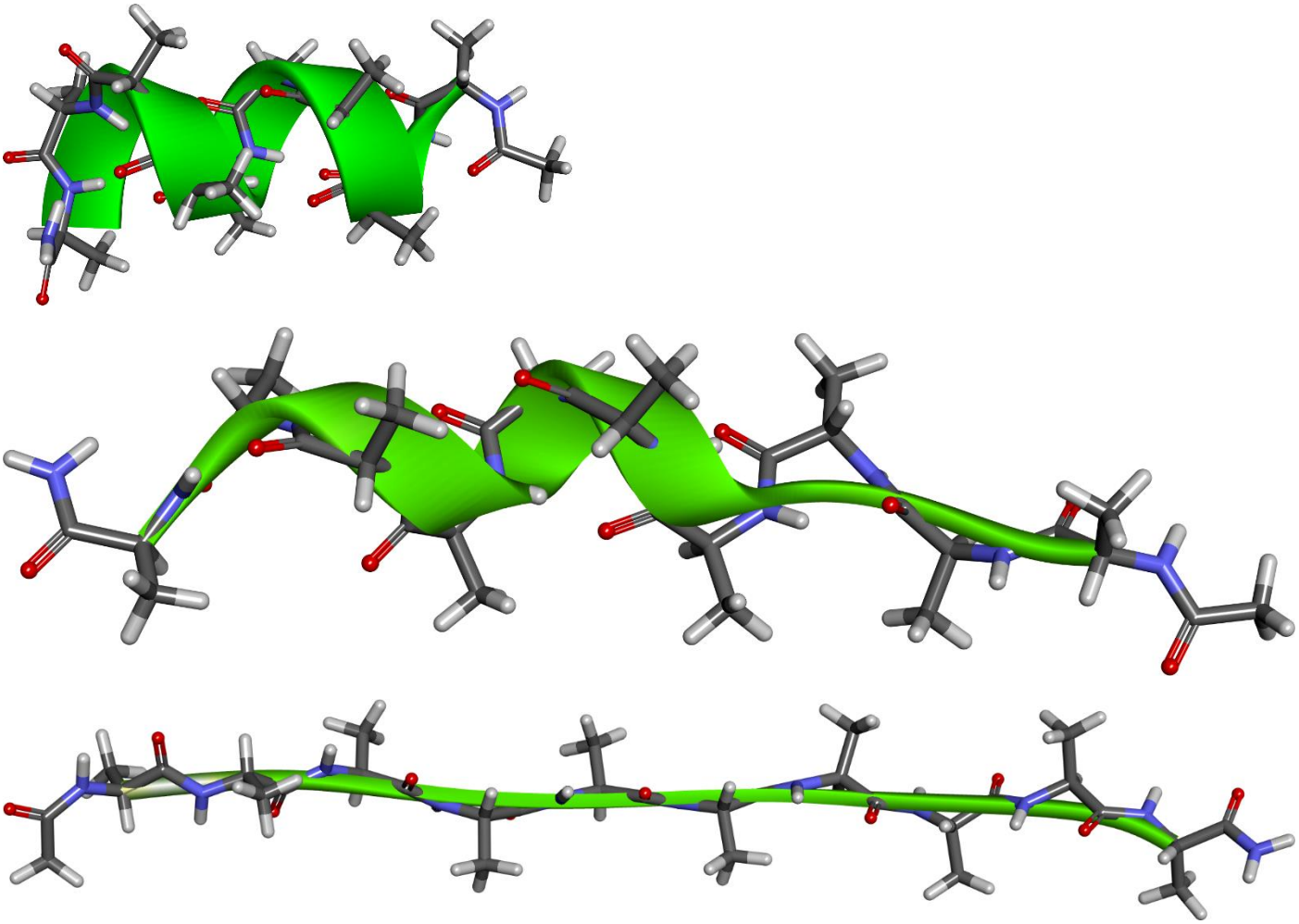

Fig. S2. Comparison between dimensionless SD profiles and overlap profiles in a-b) ACE-NME and c-d) deca-alanine. a and c give the direct free energy simulations while b and d give those in MM<->QM correction.

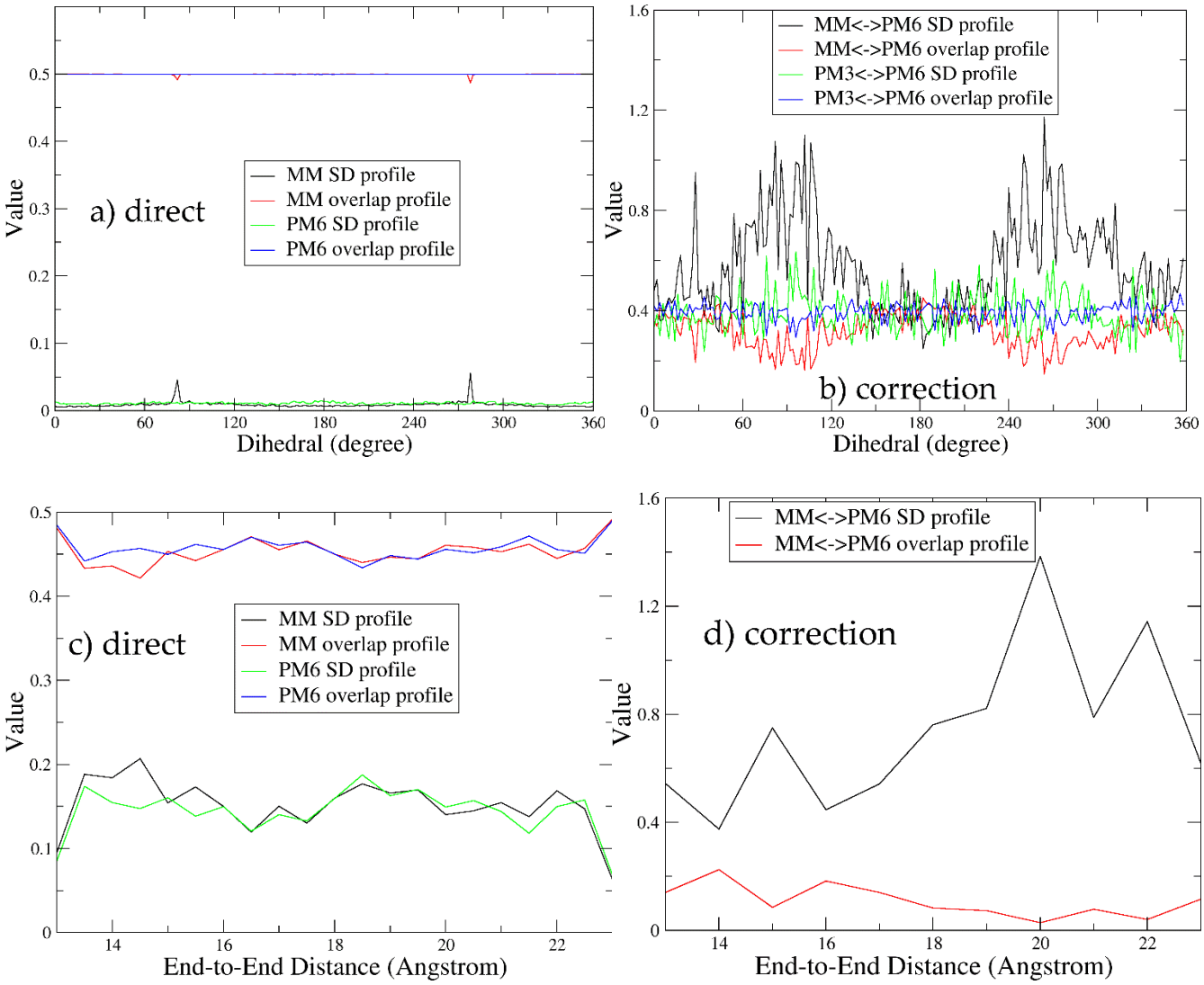

Fig. S3. The analytical result of $O_{ij} = \sigma_{ij} = \sqrt[3]{\frac{1}{2n}\left(1+\sqrt{1+\frac{32}{27n}}\right)} + \sqrt[3]{\frac{1}{2n}\left(1-\sqrt{1+\frac{32}{27n}}\right)}$.

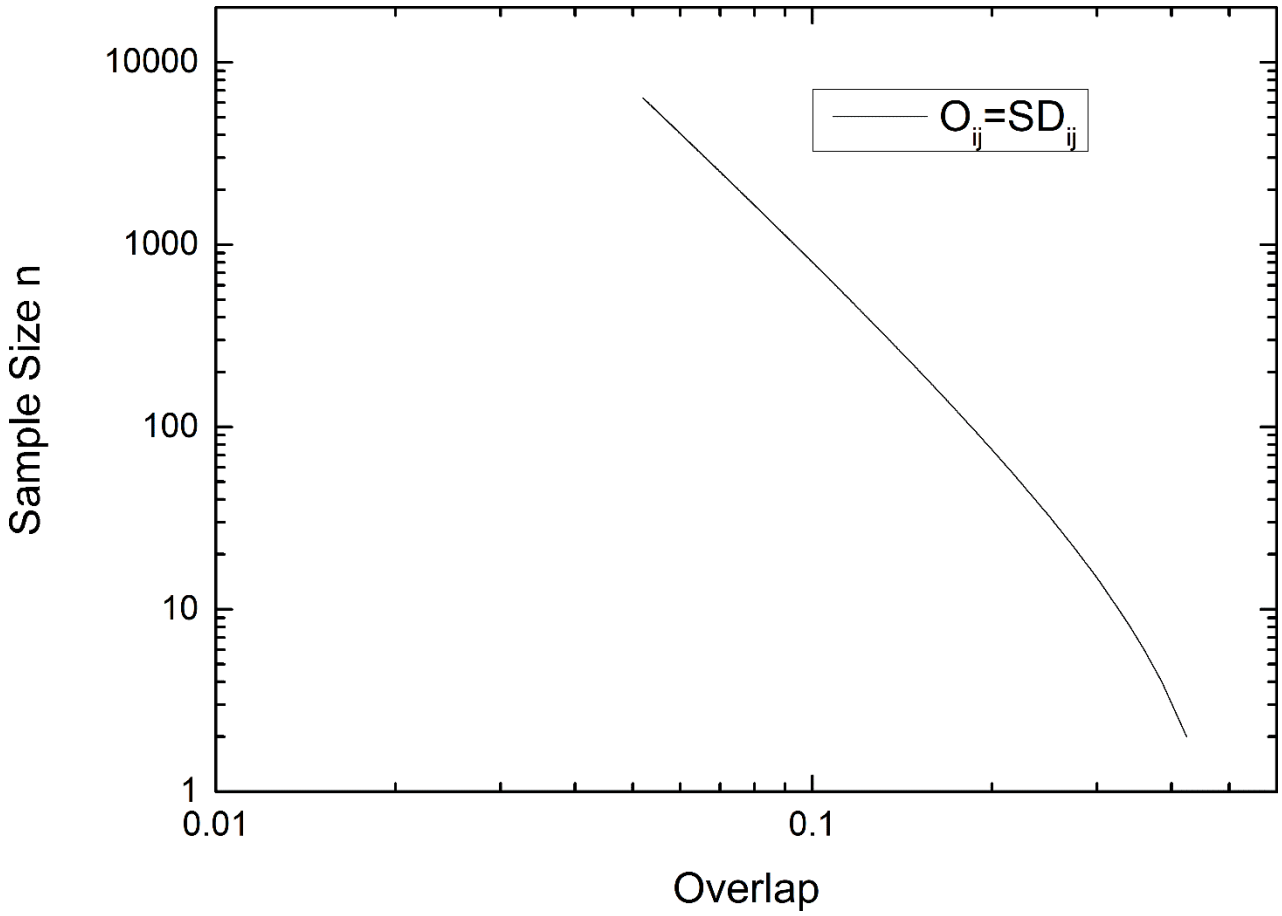

Table S1. Efficiency comparison of direct and indirect QM/MM simulation for the dihedral case. Total simulation time in direct scheme is given by $N_{\text{segments}} * N_{\text{traj}} * (\phi_{\text{NEW}} + \phi_{\text{eq}})$, while the total simulation time in the indirect scheme is the sum of $N_{\text{segments,MM}} * N_{\text{traj.MM}} * (\phi_{\text{NEW,MM}} + \phi_{\text{eq,MM}})$ at MM level and $N_{\text{traj,MM->QM}} * (\phi_{\text{NEW,MM->QM}} + \phi_{\text{eq,MM}}) + N_{\text{traj,QM->MM}} * (\phi_{\text{NEW,QM->MM}} + \phi_{\text{eq,QM}})$ in MM<->QM correction. N_{segments} is the number of segments and N_{traj} is the number of realizations per segment. The simulation time at QM level is scaled by the ratio of computational cost under QM Hamiltonian and that under MM Hamiltonian in Table 1 to be the effective simulation time at MM level, enabling direct comparison between computational costs. The computational cost of MM->PM3 differs from PM3->MM, as the initial configuration sampling procedures proceed under different Hamiltonians.

Terms / Hamiltonian	ϕ_{eq} for each initial configuration (ps)	ϕ_{NEW} in each segment (ps)	Number of segments	Number of realizations per segment	Total simulation time (ps) scaled to MM Hamiltonian	Relative efficiency
direct MM	0.05	0.5x2=1	180	25	4725.00	2.62
MM->PM3	same with MM	0.05	same with MM	3	97.79	-
PM3->MM	same with PM6	0.05	same with MM	3	141.58	-
indirect PM3	-	-	-	-	4964.37	2.50
direct PM3	0.05	0.5x2=1	180	25	12388.09	1.00